# Interannual evolution of hydrosedimentary connectivity induced by forest cover change in a snow-dominated mountainous catchment

Timothée Jautzy, Maxime Maltais, Thomas Buffin-bélanger

# Interannual evolution of hydrosedimentary connectivity induced by forest cover change in a snow-dominated mountainous catchment

**Article** *in* Land Degradation and Development · February 2021

DOI: 10.1002/ldr.3902

CITATIONS
6

READS
137

**3 authors**, including:

Maxime Maltais
Université du Québec à Rimouski UQAR
**7** PUBLICATIONS **7** CITATIONS
SEE PROFILE

Thomas Buffin-Bélanger
Université du Québec à Rimouski UQAR
**145** PUBLICATIONS **1,982** CITATIONS
SEE PROFILE

LDD Land Degradation & Development

# Interannual evolution of hydrosedimentary connectivity induced by forest cover change in a snow-dominated mountainous catchment



| | |
|---|---|
| Journal: | *Land Degradation & Development* |
| Manuscript ID | LDD-20-0718 |
| Wiley - Manuscript type: | Research Article |
| Date Submitted by the Author: | 27-Aug-2020 |
| Complete List of Authors: | Jautzy, Timothée; Université du Québec à Rimouski, Géographie<br>Maltais, Maxime; Université du Québec à Rimouski, Géographie<br>Buffin-Belanger, Thomas; Université du Québec à Rimouski, Géographie |
| Keywords: | forest cover change, hydrosedimentary connectivity, forest management, river sensitivity, index of connectivity |
| | |

# Interannual evolution of hydrosedimentary connectivity induced by forest cover change in a snow-dominated mountainous catchment

Timothée Jautzy[1*], Maxime Maltais[1], Thomas Buffin-Bélanger[1]

[1]Département de biologie, chimie et géographie, Université du Québec à Rimouski, Rimouski, Québec, Canada

Corresponding author: Timothée Jautzy, timothee_jautzy@uqar.ca

Running title: Influence of forest cover change on hydrosedimentary connectivity

**ABSTRACT (250 words)**

Hydrosedimentary connectivity is a key concept referring to the potential fluxes of water and sediment moving throughout a catchment. In forested catchments, these fluxes are prone to be altered by anthropogenic and natural disturbances. In this study, we modelled the interannual spatiotemporal evolution of hydrosedimentary connectivity influenced by forest cover change over the last four decades in the Mont-Louis catchment, a medium snow-dominated mountainous catchment in Eastern Canada, which has seen 62% of its total surface affected by forest disturbances between 1979 and 2017. Using a geomorphometric index of connectivity (IC) and a historical forest cover database, we produced one IC map per year, considering anthropogenic and natural disturbances affecting the forest cover of the studied catchment. To account for vegetation recovery, forest disturbances have been weighted with local hydrological recovery rates. In four decades, the mean IC in the Mont-Louis catchment dramatically increased by 35% in response to different types of disturbances. The spatial evolution of IC in the whole catchment and at the sub-catchment scale revealed the strong influence of the location of the disturbances on the hydrosedimentary connectivity to the main channel. The results also highlight the sharp contrast between IC computed from topography-based impedance to those computed from vegetation-based impedance. Forest disturbances appears to be prone to connect hillslopes with the hydrological network by producing pathways for sediment and water. Finally, the proposed reproducible framework might be useful to anticipate the potential impact of harvesting and prevent damages to fish habitat and sensitive river reaches.

Keywords: forest cover change, hydrosedimentary connectivity, forest management, river sensitivity, index of connectivity

[*] Present address : Laboratoire Image Ville Environnement, Université de Strasbourg, Strasbourg, France. Timothee.jautzy2@etu.unistra.fr

## 1. Introduction

The concept of hydrosedimentary connectivity, widely used in geomorphology, refers to water and sediment fluxes occurring across the landscapes over a time period (Heckmann et al., 2018; Wohl, 2017). The consideration of hydrosedimentary connectivity in catchments goes back to the beginnings of the discipline (Gilbert & Dutton, 1880), because the degree of connectivity between the landscape compartments, such as hillslopes and river channels, might explain the trajectory of geomorphic forms and processes in both space and time.

Even though fluxes of matters have been first described and qualitatively assessed for decades, their (semi)-quantification only started in the beginning of the 21st century (Wohl et al., 2019). Among the tools and indexes aiming to address hydrosedimentary connectivity that have been developed (for a review, see Heckmann et al., 2018), the index of connectivity (IC) first proposed by Borselli et al. (2008) and then recently refined (Cavalli et al., 2013; Crema & Cavalli, 2018; Trevisani & Cavalli, 2016) resulted in a flourishing series of studies proving its efficiency to (semi)-quantify hydrosedimentary connectivity in various environmental contexts and purposes (Czuba & Foufoula-Georgiou, 2015; Grischott et al., 2017; Manuel López-Vicente & Ben-Salem, 2019; Nicoll & Brierley, 2017; Prosdocimi et al., 2017).

According to Cavalli et al. (2013), IC describes *"the degree of linkage that controls sediment fluxes throughout landscapes and in particular between sediment sources and downstream areas"*. It refers to structural connectivity, which address the potential of connectivity between system components. On the other hand, functional connectivity refers to the actual fluxes of water and sediments (Heckmann et al., 2018; Wainwright et al., 2011). The advantage of the IC is that it can be computed using only a digital elevation model (DEM). Thus, the inferred connectivity depends on (i) slope, (ii) distance from source to target and (iii) a weighting factor (W) called impedance, defined as the resistance to sediment flows and runoff. The impedance is controlled by different factors related to local characteristics of the catchment such as topography and land use. Using the appropriate W then represent the most challenging part of the IC computation (Borselli et al., 2008; Cavalli et al., 2013; Zanandrea et al., 2020).

Different ways have been proposed to address the impedance. Initially, W was derived from the USLE/RUSLE C-factor (Renard, 1997; Wischmeier & Smith, 1978) to represent soil cover and potential of erosion. In the standalone software SedInConnect 2.3 developed by Crema and Cavalli (2018), a straightforward way to assess W has been implemented. It is calculated by deriving a roughness index (RI) from the DEM, based on the residual topography that considers differences between smoothed and non-smoothed terrain at a few meters scale. Other approaches emphasize on the role that land use/vegetation cover may have on the impedance, by deriving W from Manning's n (Foerster et al., 2014; Goldin, 2015; Hooke & Sandercock, 2017; Llena et al., 2019; M. López-Vicente et al., 2013; Persichillo et al., 2018). It has

also been shown that the consideration of vegetation cover in the IC is especially important in forested catchments, given that topography-based W alone is not prone to represent the strong impact of forest cover in sediment and water retention (Zanandrea et al., 2020).

Hence the necessity to use the most appropriate W, in consideration to local characteristics of the studied catchment when assessing IC, emerges as a key issue. For instance, while a topography-based W is likely to better represent the impedance in Alpine bare slopes (Cavalli et al., 2013), a land cover-based W is more adequate in vegetated catchments (Persichillo et al., 2018; Schopper et al., 2019; Zanandrea et al., 2020).

Moreover, when land use and/or vegetation cover are used to determine the impedance driving the IC, the critical issue of the dynamic state of connectivity emerges. Indeed, it is widely recognized that connectivity is prone to evolve over time, on account of topography (Calsamiglia et al., 2018; Llena et al., 2019) and especially land use/vegetation cover variations (Brierley et al., 2006; Czuba & Foufoula-Georgiou, 2015; Moreno-de-las-Heras et al., 2020; Wohl, 2017; Wohl et al., 2019), yet few studies have incorporated land use changes in the IC computation to assess its impact on the evolution of hydrosedimentary connectivity through time (Table 1). In order to evaluate the impact of land degradation on the evolution of hydrosedimentary connectivity, these studies produced diachronic land use maps and derived them into diachronic impedance maps, using either Manning's n, C-factor and satellite remote-sensed indices to eventually implement them in the IC computation.

**Table 1: Recent studies assessing the evolution of hydrosedimentary connectivity induced by land use/vegetation cover change, using IC (Cavalli et al., 2013).**

The production of diachronic land use maps usually relies on historical aerial photographs, generally acquired once a decade during the 20$^{th}$ century, limiting the frequency at which hydrosedimentary connectivity can be computed. To our knowledge, one date per ten year is the highest temporal resolution of land use maps that have been used to assess the evolution of sediment connectivity in a single catchment for periods of more than 50 years (López-Vicente et al., 2017). Thus, these studies result in semi-dynamic connectivity, as they only consider a few land use maps over longer period to quantify the evolution of connectivity. Therefore, semi-dynamic connectivity does not allow to encompass the fine spatiotemporal trajectory of connectivity induced by the historical land degradation as hydrosedimentary connectivity may be altered yearly at the scale of a watershed.

These considerations become even more relevant for forested catchments subject to frequent forest cover change induced by anthropogenic and/or natural perturbations. In the southern part of the province of Québec (Eastern Canada), most catchments have been affected by forestry for at least a century (Pinna et al., 2009), and even more intensively in the last four decades (Boucher et al., 2009). With a dense hydrological network, steep hillslopes and wide floodplains on the valley bottom, rivers of the Appalachian

Mountains are prone to be geomorphologically impacted by the potential evolution of the hydrosedimentary connectivity induced by historical forest cover changes.

Taking advantage of a detailed historical forest cover database covering almost four decades produced by the Minister of Forests, Wildlife and Parks (MFFP, 2018), this study aims to precisely quantify the spatiotemporal evolution of hydrosedimentary connectivity induced by forest cover change in the Mont-Louis catchment, a medium (~300 km²) snowmelt-dominated forested watershed located in the northernmost part of the Appalachians mountains. The originality of this study lies in the fact that we compute the yearly evolution of hydrosedimentary connectivity over the last four decades, from a set of 38 forest disturbance maps (FDM), rather than a quasi-dynamic connectivity from a few land use maps. First, the FDMs are translated into 38 W rasters according to local hydrological recovery (HR) rates assessed by Plamondon et al. (2004; 2002), which accounts for canopy height/density, basal area, disturbance type and snowmelt rate, as vegetation regrows (Talbot et al., 2006; Zhang et al., 2012). Then, the yearly evolution of hydrosedimentary connectivity in the Mont-Louis catchment is computed using the IC proposed by Cavalli et al. (2013), in which W rasters are implemented as a dynamic impedance.

In this paper, we propose that historical forest cover change imply a (i) temporal evolution and (ii) spatial variability of hydrosedimentary connectivity and present illustrations supporting these propositions. This study also demonstrates that an accurate portrait of the spatiotemporal evolution of the IC can be easily depicted at the catchment scale, and that our workflow can be used as an efficient tool to better understand how forest cover change impacts hydrosedimentary connectivity, in space and time.

## 2. Study area

The Chic-Chocs range is located in the northeastern part of the Appalachians mountains, in the Gaspé Peninsula, Quebec, Canada. The Appalachians were forms by three orogenesis, resulting in an extensively deformed shale and limestone structure (Hétu & Gray, 1980). The Mont-Louis watershed drains about 300 km² on the northern part of the mountain range, the catchment's headwater reaches over 900m in altitude and the 45 km river flows north down to the Saint-Lawrence river (Figure 1). The upstream reaches of the river are mostly confined within steep hillslopes, canyons and a bedrock bed (slope ~ 0,017). As the valley widens and the slope decreases (0,0025), a wide floodplain (≈400 m) appears, alongside with Holocene deposits in the valley bottom.

Since the first settlements in the XVIII$^{e}$ century, the whole Gaspé Peninsula has been increasingly exploited for its wood resources (Boucher et al., 2009). In the Mont-Louis catchment, the first major logging company, the *Mont-Louis Seigniory* has been operating from 1924 to 1958 (Pelletier, 2014). Other companies have been conducting logging activities in the catchment since then, but they only started in the mid 1990's (MTES, 2020).

A qualitative assessment of historical aerial photographs reveals that in 1963, most of the catchment was covered with mature forest. Only a few minor cuts could be identified and vegetation cover data from 1979 (MFFP, 2018) shows that disturbances were still low. It thus indicates that between the *Mont-Louis Seigniory* operations and the most recent period of logging (mid 1990's), forest cover was mostly mature throughout the catchment and that the intensified logging beginning in the 1990's massively degraded the forest cover. Throughout the study period (1979-2017) more than 60% of the catchment's surface has been affected by natural (wildfires, insects, diseases) or anthropogenic anthropic (logging, thinning, plantations) disturbances.

**Figure 1. Mont-Louis catchment location. a) Mont-Louis topographic map and sub-catchments. b) Gaspé peninsula and Mont-Louis catchment location. c) Gaspé peninsula location in Canada.**

## 3. Material and methods

### 3.1. Forest disturbance maps production

The forest cover changes in the Mont-Louis watershed have been characterized using a highly detailed spatiotemporal database from the fifth Ecoforestry Inventory (EFI). It is carried out every 10 years to produce a set of maps depicting an accurate portrait of the forest's state, all over the Southern part of Quebec (MFFP, 2018). This inventory is updated yearly and describes the types of forest stands according to their species, the density and the age and height of the stands. These data are produced by aerial photographs interpretation with a spatial resolution of 30cm.

In addition to the stand's characteristics, both anthropogenic (logging/reforestation) and natural (wildfires, insects, diseases) forest disturbances are annually mapped since the early 1970's. Wildfires are mapped from satellite imagery, insects and diseases are mapped from a combination of satellite imagery, aerial surveys along with aerials photographs and anthropogenic disturbances are mapped through the collaboration of several stakeholders related to the agroforestry industry during field surveys. Because the types of disturbances will be considered in the computation of the IC, it is worth noting that there are up to 50 different harvest types and reforestation operations occurring in Quebec. These disturbances range from clear-cutting and partial cuts to commercial thinning and plantations.

These spatial data are publicly available in GIS format since 2017. We merged them in a single shapefile of overlaying polygons and clipped to Mont-Louis catchment boundaries. Each polygon represents a single disturbance two attributes have been used in this study: year of occurrence (Figure 2a) and type of

disturbance. In Mont-Louis catchment, the first recorded disturbance occurred in 1979. In 2017, 63 % of the catchment area has been affected by disturbances.

**Figure 2: Processing of the spatiotemporal ecoforestry database. a) Example of the 2016 forest disturbance map (FDM) resulting in the b) 2016 impedance raster ($W_{HR}$), with a zoom-in illustrating c) the high spatial resolution of $W_{HR}$, which depends on the different types of disturbances (1-5), and d) the associated orthophoto (2016).**

Then for the study period (1979-2017), an annual time series of FDM (Figure 2a) is extracted from the raw shapefile. Each FDM corresponds to the cumulated disturbances that took place in the catchment from the first year (1979) to the considered year. When several disturbances occur at the same location, only the latest is considered.

### 3.2. Yearly connectivity computation

#### 3.2.1. Index of connectivity

The computation of hydrosedimentary connectivity maps is performed using the software SedInConnect 2.3 (Crema & Cavalli, 2018), which computes the IC as defined by Cavalli et al. (2013):

$$IC = \log_{10}\left(\frac{D_{up}}{D_{dn}}\right)$$

where $D_{up}$ and $D_{dn}$ are the upslope and the downslope component, respectively.

$D_{up}$ corresponds to the potential for downward routing of the sediment produced upslope. It is expressed as follows:

$$D_{up} = W\,S\,\sqrt{A}$$

where W corresponds to the impedance factor (i.e. the resistance to runoff and sediment flow; dimensionless), S is the slope (%) and A is the contributing area ($m^2$).

$D_{dn}$ considers the flow path length that a particle must travel to reach the nearest sink or target. It is expressed as follows:

$$D_{dn} = \sum_i \frac{d_i}{W_i S_i}$$

where $d_i$ is the length of the flow path along the $i^{th}$ cell according to steepest downslope direction (m), $W_i$ and $S_i$ are the impedance and the slope gradient of the $i^{th}$ cell, respectively.

SedInConnect 2.3 require a DEM as a minimum input. We used a single 10 m DEM and selected the Mont-Louis river main channel as the target (Figure 1). The DEM has been filled to remove local depressions and to ensure continuity of the flow path lines. The computed IC then represent the connectivity to the main channel. As for the impedance factor, the software proposes to compute it directly from the DEM (topography-based) as a surface roughness index ($W_{RI}$), following the approach of Cavalli et al. (2013). The software also allows the user to define its own W raster.

While the topography-based impedance factors generally lead to static connectivity, it has been shown that connectivity can be highly dynamic over time, especially when considering land use/forest cover change (Llena et al., 2019; Moreno-de-las-Heras et al., 2020; Ortíz-Rodríguez et al., 2019; Poeppl et al., 2017). Thus, to best evaluate the effect of forest cover change on connectivity, this study implement a highly dynamic impedance factor in the IC computation, based on hydrological recovery rates.

#### 3.2.2. Hydrological recovery as a dynamic impedance factor

In Québec (eastern Canada), as in western Canada and in the United States, eco-forestry data are used to estimate the equivalent cut area (ECA) affecting watersheds, in order to achieve forests sustainable management objectives (Ager & Clifton, 2005; B.C. Ministry of Forests, 2001; Langevin & Plamondon, 2004). The ECA is an index that combines multiples types of forest disturbances and considers vegetation recovery. To date, ECA is considered the best index to assess cumulative forest disturbance effects on hydrology (Ning et al., 2017; Wei et al., 2016; Wei & Zhang, 2011; Winkler et al., 2017), especially in large watersheds. It has been successfully used to demonstrate that cumulative forest disturbances can significantly increase the annual runoff (Giles-Hansen et al., 2019; Li et al., 2017; Zhang et al., 2016, 2017). ECA is defined as the area that has been anthropically or naturally disturbed (logging, wildfire, insect invasions), weighted by a local factor called hydrological recovery (HR). The latter accounts for canopy height and density, basal area (related to tree heights and/or disturbance date), snowmelt rate and depends also on the type of disturbance. HR generally varies from 0%, basically representing a recent clear-cut, to 100%, representing a hydrologically recovered forest stand or an unlogged mature forest (Winkler et al., 2017).

Plamondon (2004) assessed the HR rates suitable to snow-dominated resinous Quebec forests, by deriving HR rates from snow augmentation coefficient (SAC; equation 1), which is estimated using relationships between forest stand characteristics and snowmelt rate, as vegetation regrowth (Hudson, 2000; Langevin & Plamondon, 2004; Talbot et al., 2006; Talbot & Plamondon, 2002; Zhang et al., 2012).

SAC = 100% - HR (equation 1)

The SAC varies from 0% (when HR=100%) to 100% (when HR=0%).

**Figure 3: Temporal evolution of the impedance ($W_{HR}$) used in this study, depending on disturbance age, category and tree height. Values of impedance are directly derived from the snow augmentation coefficient rate (SAC) established by Langevin and Plamondon (2004).**

We argue that the use of the SACs established by Plamondon (2004) as the impedance factor in the computation of the IC in a snow-dominated forested watershed is a relevant choice, for three reasons. First, as recommended by Cavalli et al. (2013), the SAC (i) preserves the dimensionless aspect of the IC (Martini et al., 2020) and (ii) displays a large distribution of its values from 0 to 1 (Figure 3). The importance of a large distribution of W values, especially when studying the role of forest cover in the IC, has been recently emphasized by Zanandrea et al. (2020).

Secondly, as the Mont-Louis watershed is almost exclusively covered by forest, the use of the SAC, which is directly related to forest stand characteristics, might better represent the influence of the forest cover than Mannings' n for instance, when addressing hydrosedimentary connectivity.

Last but not least, the SAC is highly dynamic as it evolves yearly with vegetation regrowth (Figure 3). Thus, it better represents the temporal evolution of the impedance induced by the forest cover changes and stands recovery. Furthermore, depending of the type of disturbance, different HR rates are used. Langevin and Plamondon (2004) defined six categories of disturbances. For instance, forest stands affected by a disturbance from the 5$^{th}$ category (e.g. commercial thinning) are considered to recover their initial hydrological characteristics after seven years, while forest stands affected by disturbances from the 1$^{st}$ (e.g. clear-cut) or the 6$^{th}$ category (e.g. insects disease) recover their initial hydrological characteristics after 35 years (Figure 3).

To implement SACs as the impedance factor in IC computation, an annual time series of 38 W rasters (Figure 2b) is derived from the FDM maps (Figure 2a). The 10 m pixels of the W rasters are affected with the SACs values ranging from 0.001 to 1, according to Figure 3. Following Ortiz-Rodriguez et al. (2019) approach and because W must be different from zero, pixels covering undisturbed areas are affected with a W value of 0.001 (Figure 2b-c). Maps of connectivity, hereafter called $IC_{HR}$, are computed annually from 1979 to 2017, with the single 10 m DEM and the associated W rasters, hereafter called $W_{HR}$ (HR referring to the consideration of the hydrological recovery rates).

To evaluate the effects of dynamics $W_{HR}$ on hydrosedimentary connectivity, we also computed ICs using a uniform impedance ($W_1$; Zanandrea et al., 2020) and a topography-based impedance ($W_{RI}$; Cavalli et al., 2013).

Given the large dataset of time-series IC maps produced with our methodology, results are presented by emphasizing on (i) the spatial effects of forest cover changes on IC, (ii) the temporal effects of forest cover changes on the evolution of IC and (iii) the spatiotemporal patterns of IC emerging from forest cover changes.

## 4. Results

### 4.1. Comparison of IC spatial distribution from topography-based ($W_{RI}$) and vegetation-based ($W_{HR}$) impedances

The distributions of $IC_{RI}$ and $IC_{HR}(2017)$ values and their spatial distribution are presented in figure 4 and 5a-c, respectively. We use $IC_{HR}(2017)$ as a reference since it is the most recent computed $IC_{HR}$ map. To evaluate the effects of $W_{RI}$ and $W_{HR}(2017)$, $IC_1$ - computed using a uniform impedance of 1 - is also shown. To highlight the spatial effects of using different impedances on IC calculation, the maps and violin boxplots are color-scaled using 8 quantiles (Calsamiglia et al., 2018; Crema & Cavalli, 2018; Llena et al., 2019).

The distributions of $IC_1$ and $IC_{RI}$ values are identical (KS test statistic = 0.011; p-value < 2.2e-16), with respective median values of -4.37 and -4.39 (Figure 4). This similarity is also reflected in the spatial distributions of $IC_1$ and $IC_{RI}$ (Figure 5a-b) that are both exposing relatively simple patterns of connectivity, the most obvious one being dictated by the proximity of the channel. The $IC_{HR}$ shows high values near the channel and lower values further away. Second is a longitudinal decreasing trend, as the level of connectivity appears to be much higher and homogenous in the upper part of the catchment and lower or discontinued downstream. This result suggests that, even when using the roughness index as impedance ($W_{RI}$), the IC remains mainly controlled by the slope and the distance to the target, i.e. the main channel. Here, the high similarity between $IC_1$ and $IC_{RI}$ also reveals the irrelevance of the RI in our study.

Using vegetation-based impedance ($W_{HR}(2017)$) significantly reduces the overall distribution of IC values (median = -8.20), emphasizing the strong influence of the forest cover on water and sediment retention (Figure 4). Moreover, the consideration of the forest cover seems to disconnect valley hillslopes from channels but connect more remote areas (Figure 5c). As a result, the pattern of connectivity appear more complex and heterogeneous for $IC_{HR}(2017)$ than those of $IC_1$ and $IC_{RI}$. Finally, the impact of vegetation on IC is spatially variable (Figure 5d). The absolute difference between $IC_{RI}$ and $IC_{HR}(2017)$ highlight that the most impacted parts are in the middle-west of the catchment, while hydrosedimentary connectivity of the downstream parts seem to be less affected by vegetation cover.

**Figure 4: Violin boxplots of IC values over the Mont-Louis catchment, computed with three impedances ($W_1$, $W_{RI}$, $W_{HR}(2017)$).**

**Figure 5: IC maps depending on the impedance. a) Uniform impedance ($W_1$). b) Topography-based impedance ($W_{RI}$). c) Vegetation-based impedance ($W_{HR}(2017)$). d) Absolute difference between $IC_{HR}(2017)$ and $IC_{RI}$.**

The impact of vegetation on spatial patterns of connectivity can be highlighted at the sub-catchment scale. Figure 6 focuses on three sub-catchments (14,15,16) and shows the decoupling/coupling effect of the presence (absence) of vegetation on the hydrosedimentary connectivity. While the first series of maps ($IC_{RI}$) display patterns of connectivity mainly topography-controlled, the second series of maps ($IC_{HR}(2017)$) display reversed patterns, with their upstream part coupled to the main channel and their downstream part globally decoupled, due to the harvested areas upstream and mature forest downstream.

**Figure 6: Comparison of IC in three sub-catchments (14,15,16) when computed with $W_{RI}$ and $W_{HR}(2016)$. The 2016 orthophoto reflects the importance of considering the presence (absence) of vegetation.**

To explore further the role of the vegetation on IC through the Mont-Louis catchment, Figure 7 plots the distributions of standardized $IC_{RI}$ and $IC_{HR}(2017)$ for every sub-catchment. The use of a vegetation-based impedance generates wider ranges of IC values for almost all sub-catchment as revealed by the mean IQR values of $IC_{HR}(2017)$ (1.36) twice those of $IC_{RI}$ (0.67). These wider ranges reflect the spatially variable impact of forest cover consideration over each sub-catchment.

For instance, every sub-catchment (except 2, 3 and 10) display a lower mode in $IC_{HR}(2017)$ distribution, suggesting that a part of the catchment has seen its connectivity reduced by the consideration of the forest cover (decoupling). By contrast, some catchments (e.g. 10-13 and 16) display a higher mode in $IC_{HR}(2017)$ distribution, suggesting that a part of the catchment has seen its connectivity increased by forest cover degradation (coupling).

**Figure 7: Distribution of standardized IC values depending on the impedance ($W_{HR}$ and $W_{RI}$), extracted from each sub-catchment.**

### 4.2. Interannual evolution of IC using a vegetation-based impedance ($W_{HR}$)

Figure 8 summarizes the interannual evolution of IC using the vegetation-based impedance from 1979 to 2017 in the Mont-Louis catchment. In Figure 8a, the $IC_{HR}$ mean value is shown within the theoretical range (max, min) of IC mean value that is being computed using uniform impedance of 1 ($W_1$) and 0.001 ($W_{0.001}$) for max and min, respectively. The standard deviation evolution has been plotted on a distinct vertical scale (Figure 8b) to better visualize the associated trend. Figure 8c displays the distribution of $IC_{HR}$ values over three distinct years, 1979, 1994 and 2012 (black highlighted points in Figure 8a-b), respectively. They are representative of how the distribution of $IC_{HR}$ values evolves in time. The entire time-series of $IC_{HR}$ maps is available online in Supporting Information (Figure S1).

Figure 8 suggests that $IC_{HR}$ is highly dynamic in time, as displayed by the evolution of the mean, standard deviation, and distribution of $IC_{HR}$. The mean $IC_{HR}$ temporal evolution (Figure 8a) reveals that the hydrosedimentary connectivity globally increases over the period. The minimum and maximum value occurs in 1979 and 2012 with values of -10.22 and -8.13, respectively. This corresponds to a significant increase of 35%, according to the theoretical maximum range. The $IC_{HR}$ temporal trajectory can be divided in three phases. First, from 1979 to 1993, the connectivity increases in three marked steps, in 1981, 1986 and 1989. Then, from 1989 to 1993, IC displays a slight decrease. The second phase of the trajectory corresponds to a constant increase from 1994 to 2005 (except a discontinuity in 2000). Finally, connectivity reaches a plateau where mean $IC_{HR}$ is roughly constant from 2006 until 2015 where $IC_{HR}$ starts to decrease. As for the standard deviation of IC values over Mont-Louis catchment (Figure 8b), its trajectory displays a decreasing trend from 1986 to 2017, after having drastically increased in 1981.

**Figure 8: Temporal evolution of IC over Mont-Louis catchment, from 1979 to 2017. a) Mean value of $IC_{HR}$. Black dashed lines corresponds to the theoretical maximum and minimum possible value of the mean $IC_{HR}$. b) Standard deviation of $IC_{HR}$. c) $IC_{HR}$ distributions for year 1979, 1994 and 2012.**

### 4.3. Spatiotemporal trends

Figure 9 maps the distribution moments of the $IC_{HR}$ time series to expose elements of the spatiotemporal variability of the hydrosedimentary connectivity. The maps allow to identify where within the watershed the $IC_{HR}$ has been on average high or low (Figure 9a-b), has been highly variable (Figure 9c) and has presented punctual but significant spikes (Figure 9d) during the studied time period. For example, it can be

seen that the $IC_{HR}$ is in general higher along the Mont-Louis river in the middle part of the watershed (mean and median values) and that the $IC_{HR}$ values are relatively stable over time because of low standard deviation values. The distribution moments, however, are not sufficient to get a clear picture of the spatiotemporal trends and a better representation is needed.

**Figure 9: Spatiotemporal trends over the time-series of $IC_{HR}$ from 1979 to 2017. a) Mean $IC_{HR}$. b) Median $IC_{HR}$. c) $IC_{HR}$ standard deviation. d) $IC_{HR}$ skewness.**

Figure 10 gives a detailed overview of the interannual evolution of the hydrosedimentary connectivity, at the catchment scale. Mean $IC_{HR}$ has been extracted per individualized sub-catchments (Figure 10a) and per cumulated sub-catchments (Figure 10b). The latter corresponds to the whole drainage area of each sub-catchment outlets. Thus, it refers to the longitudinal evolution of the mean $IC_{HR}$ along the main channel. These two visualization approaches are complementary, as they allow to observe the spatiotemporal evolution of $IC_{HR}$ at two different spatial scales, the sub-catchments themselves and along the main channel, respectively.

By emphasizing on individualized sub-catchments (Figure 10a), three major observations can be made about Mont-Louis spatiotemporal evolution of hydrosedimentary connectivity. First, while all individualized sub-catchments display an increasing trend of mean $IC_{HR}$, this increase occurs in contrasting ways. For instance, some sub-catchments (3-6) experienced a rapid and stepped increases of mean $IC_{HR}$, while others (2, 12-16) display a smaller yet continuous increase of the mean $IC_{HR}$. In the most recent period, some sub-catchments (1, 7, 9, 10) even show a slight decrease as vegetation recovers. Second, a global temporal shift in mean $IC_{HR}$ occurs around 1990 where almost every sub-catchment sees its mean $IC_{HR}$ exceeding -10. This allows us to suggest two main temporal periods in hydrosedimentary evolution. Third, as mentioned (see part IV.b), there is a general trend toward the augmentation in $IC_{HR}$ since the mid 1990's. This is even more obvious in sub-catchments 1 to 10, where not only are IC values at their highest but also where the increase of IC has been sharp and sudden. The upstream and downstream parts of the catchment therefore represent two distinct zones that will be discussed later.

The evolution of $IC_{HR}$ in cumulated sub-catchments (Figure 10b) makes it possible to visualize the spatiotemporal evolution of mean $IC_{HR}$ in Mont-Louis catchment in a different way, i.e. the longitudinal evolution of $IC_{HR}$ along the main channel. While this approach globally confirms the observations made from Figure 10a (i.e. two main temporal periods and two distinct spatial zones), it also emphasizes the possible role of the size of the sub-catchments on the longitudinal evolution of $IC_{HR}$ along the main channel. Indeed,

it appears clearly that the biggest sub-catchment (i.e. 12) causes a longitudinal discontinuity in mean $IC_{HR}$ along the main channel, by drastically decreasing $IC_{HR}$ value, regardless of the year. This suggest that the 12$^{th}$ sub-catchment has a strong influence in the intensity of the average hydrosedimentary connectivity to the main channel, most certainly due to its large size.

**Figure 10: Spatiotemporal matrix of mean $IC_{HR}$ computed per a) individualized and b) cumulated sub-catchments.**

## 5. Discussion

### 5.1. The role of the forest cover dynamics on the evolution of hydrosedimentary connectivity

Our comparison of the influence of topography based ($W_{RI}$) and vegetation based ($W_{HR}$) impedances on the IC validate the premise regarding the lowering effect of forest cover on hydrosedimentary connectivity (Zanandrea et al., 2020). While $IC_{RI}$ and $IC_1$ have identical distributions (Figure 5), $IC_{HR}$ shows lower values and a greater range, confirming that forest cover globally decreases the level of connectivity throughout the catchment. Moreover, the values of $IC_{HR}$ are more spatially heterogeneous than those of $IC_{RI}$. This spatial variability is likely due to forest disturbances occurring on various parts of the catchment, eventually followed by vegetation recovery that dims the effects of the initial disturbances. If some parts of the catchment tends to be coupled or decoupled to the main channel by forest disturbances or presence (Figure 5;6), some others are not as sensitive, which reveals that IC is not exclusively controlled by forest cover. For instance, the upstream part of the catchment is highly connected to the main channel, whether the $W_{RI}$ or the $W_{HR}$ is used as impedance, and vegetation seems to have very little impact on the level of connectivity (Figure 5). This highlights that in this specific location, connectivity is likely topography controlled. On the other hand, other areas such as the inset in Figure 5 display very low connectivity when using $W_{RI}$ but a higher connectivity when using $W_{HR}$. In these areas, slopes are more gentles and topography itself is insufficient to dictate the level of connectivity, indicating that hydrosedimentary connectivity is likely vegetation controlled.

Although it is widely known that connectivity is temporally dynamic (Czuba & Foufoula-Georgiou, 2015), there is yet a lack of analysis at a temporal resolution allowing the emergence of fine spatiotemporal trajectories. Most studies using the IC to address its temporal evolution are using either C-factor, Manning's n or satellite remote-sensed indices as impedance in order to compute the IC (Table 1), resulting in a semi-dynamic connectivity portrait, which can be an issue for two reasons. Either only a few dates have been used to cover few decades (e.g. Lizaga et al., 2018; López-Vicente et al., 2017; Persichillo et al., 2018), giving

an incomplete or flawed understanding of the way IC evolved through time, or multiples dates have been used to compute IC over relatively short period of time (Foerster et al., 2014; Ortíz-Rodríguez et al., 2019), providing a very limited scope and a lack of context to understand the global evolution of the connectivity (Czuba & Foufoula-Georgiou, 2015). There is thus a real need of increasing the temporal resolution to allow emergence of spatiotemporal trajectories (Nicoll & Brierley, 2017).

In this study, we propose a method that address both these issues. Compared to previous studies (Table 1), our framework increases the frequency at which IC is computed from decades to years, hence increasing the temporal resolution and allowing to appreciate the whole trajectory of the hydrosedimentary connectivity. In Mont-Louis Catchment, three phases have been identified. The first one occurs between 1979 and 1993, where IC increases in marked steps. These steps are controlled by the sudden occurrence of three insect outbreaks affecting areas between 9 and 20 $km^2$, mostly close to the channel. The second phase occurs between 1994 and 2005, where a gradual increase of IC occurs, due to a regular succession of harvested areas of less than 10 $km^2$ and a greater spatial heterogeneity than the insect outbreaks. Finally, the last phase (2006-2017) is characterized by a plateau and the initiation of a decreasing trend since 2015. This is likely due to the combined effect of vegetation regrowth and stabilisation in the total harvested surface.

It is worth noting that while the use of few dates to address the hydrosedimentary connectivity would have identified the global increasing trend of connectivity throughout the Mont-Louis catchment (black points; Figure 8a), it would still lacks details on the way this process happened, as it does not account for the distinct behavior of the three periods, and mostly, it doesn't grasp the decreasing trend that is most relevant to fully understand what is currently happening in the watershed and the relevance of future projections. This is specifically what makes the interannual hydrosedimentary connectivity index a potential tool to understand how connectivity's dynamic impacts the river's dynamic and to make enlightened decisions regarding land use and development.

### 5.2. Perspectives and limitations of interannual evolution of hydrosedimentary connectivity for forest management

In North America in terms of forest management, the commonly used index accounting for vegetation state and recovery is the ECA (Winkler et al., 2017). Its main purpose is to assess the cumulated effects of past and current forest disturbances on the water yield and quality. The percentage of ECA is often used as a threshold in terms of harvested area in a catchment, generally to avoid fish habitats to be disturbed. For instance, the MFFP (Quebec) limits the ECA at 50% for any Atlantic salmon river watershed (MFFP, 2018;

Plamondon, 2004). In British Columbia, the threshold is set between 20 and 30% depending on the type of watershed (B.C. Ministry of Forests, 2001; Winkler et al., 2017). However, one of the main limit of the ECA is the lack of consideration of the disturbance positions (Pike et al., 2010; Wei & Zhang, 2011), as ECA index does not account for the distance of the disturbance to the channel, neither for the slope.

While using the same indicator of vegetation recovery (i.e. HR) as the ECA, the proposed methodology integrates HR as the impedance in the computation of a highly used connectivity index (IC). It provides a better picture of the catchment hydrosedimentary sensitivity as well as its evolution in retrospective time. More interestingly, however, the methodology could allow to determine the extent to which prospective forest harvest may increase the overall hydrosedimentary connectivity at the scale of the catchment but also within sub-catchments by integrating the known location and dimension of prospective harvests in the computation of IC maps. Furthermore, combined with specific information on the location of fish habitats, and the characteristics of the main channel, the resulting maps may highlight river reaches that are more likely to be affected by the change in IC resulting from forest disturbances. As a result, the integration of the HR as the impedance in the IC computation might challenge the use of a fixed threshold of ECA in forestry, by proposing a different picture of a catchment based on the IC. This might be implemented in river sensitivity analysis to explain historical river adjustments and to expose potential river changes (Lisenby et al., 2019).

Sensitivity, as a geomorphic concept, refers to the adjustability of a landform or a process to environmental disturbances (Fryirs, 2017). For river systems, more sensitive river reaches are those that are likely to adjust to a local or regional perturbation whereas those that are less sensitive are those that are likely to keep their characteristics over time. At the scale of a watershed, more sensitive and less sensitive river reaches coexist so that heterogeneity in adjustment will occur across the river system. A challenge is to provide tools and framework to support river sensitivity analysis at the scale of a watershed (Lisenby et al., 2019). It has been recognized that sediment connectivity along a river network control the location, number, form and severity of river channel changes to regional perturbation (Czuba & Foufoula-Georgiou, 2015; Lisenby et al., 2019). The workflow proposed in this study, generates interannual hydrosedimentary connectivity indices leading to maps and representation tools that allow to locate river reaches likely to sustain morphological adjustments due to significant longitudinal or temporal change in hydrosedimentary connectivity. Combining this information with geomorphological trajectories of river reaches will then allow to determine the sensitivity of the reaches to upstream changes in hydrosedimentary connectivity related to forest harvesting or degradation.

Figure 11 summarizes the complete workflow we used to assess the inter-annual evolution of hydrosedimentary connectivity using FDMs. The simplicity of the workflow reflects the relative ease to produce multi-temporal IC maps, using data that is generally available all around the world. This may

encourage researchers and forest managers to apply it in their areas of study. It requires multi-temporal FDMs, ideally from a historical forestry database, tabulated impedance suited to the study area, and a DEM. Thus, our framework would be (i) easily transferrable to any forested watershed covered by detailed spatial historical records on disturbance types (e.g. BC, Alberta and US) and (ii) most likely transferrable to forested watershed non covered by detailed spatial historical records, with an adapted indicator of historical forest change, NDVI for instance (Aires et al., 2020; Martini et al., 2020; Ning et al., 2017), which might be converted into tabulated impedance.

**Figure 11: Synthetic workflow used to assess the interannual evolution of IC using FDMs, tabulated impedances and a DEM.**

Finally, some considerations of the proposed framework must be discussed. First, there is a need to consider the temporal window that is used when computing the HR values for the first few years of the time series. In our case, the first recorded forest disturbance in the Mont-Louis watershed was in 1979. Although forest history of that area suggests no disturbance occurred prior to that date, it could be the case that a significant disturbance in 1970, for example, was not officially recorded. As a result, the computation of the HR for that area could be underestimated at the beginning of the time series as would be the computed hydrosedimentary connectivity. Secondly, although the IC is a straightforward indicator for hydrological connectivity, it remains a potential connectivity as far as sediments are concerned. To fully address sediment mobility, there is a need to use both IC and geomorphic analysis to define actual sensitivity of river reaches. Integrating geomorphic features, such as lakes and alluvial fans, as well as quaternary deposits within the watershed into the analysis constitute a promising avenue to improve our understanding of sediment availability and mobility that could lead to sensitivity of river reaches (Nicoll & Brierley, 2017).

## 6. Conclusions

The choice and effectiveness of the impedance is one of the most challenging aspect of the IC computation and vegetation has long been recognized to influence hydrosedimentary connectivity, in space and time. Yet, very little work has been done to integrate vegetation dynamic in such a model, even though it is considered crucial to improve river management.

In this study, a detailed historical forest cover database was used to implement a highly dynamic impedance in the computation of the IC. It appears that the integration of local HR as an evolutive impedance is an

efficient way to model the interannual evolution of the hydrosedimentary connectivity in a forested catchment.

On top of validating the fact that RI is not suited to model the impedance in a vegetated catchment, our study provides new inputs in the comprehension of the effects of forest cover change on IC dynamic at a high spatiotemporal resolution.

First, the use of vegetation-based impedance reveals that the hydrosedimentary connectivity in a catchment can be very sensitive to the location of the forest disturbances. The presence (absence) of vegetation can induce dramatic decoupling/coupling effects on hillslopes, potentially enhanced by topography. Such effects drastically complexifies the IC patterns at multiple scales within the catchment.

Second, the use of interannual forest cover data allows to define the complete trajectory of the hydrosedimentary connectivity over decades, which is a major step in the establishment of an accurate portrait of the spatiotemporal evolution of the IC at a catchment scale.

We argue that the combination of high spatial and high temporal resolution of IC (Figure 10) could help forest managers to plan appropriate decisions by considering hydrosedimentary sensitivity when anticipating harvests. In that regard, the proposed workflow might be used as a tool. However, further research may also consider the availability of sediments and geomorphic sinks in the catchment to establish the actual hydrosedimentary fluxes. Such knowledge could eventually lead to river sensitivity analysis at a high spatiotemporal resolution.

**Acknowledgements**: This work was funded by the Ministry of Public Safety of Quebec (grant no. CPS 18 19 03) and by an NSERC Discovery grant (T. Buffin-Bélanger; grant no. 298125). We warmly thank Frédérique Dumont and Alexia Désormeaux for their help with the forest cover database processing.

**Conflict of interest statement:** The authors declare no conflict of interest.

**Data availability statement:** The data used in this study are publicly available.

Quebec ecoforestry inventory: https://mffp.gouv.qc.ca/le-ministere/acces-aux-donnees-gratuites/

SedInConnect 2.3: https://github.com/HydrogeomorphologyTools/SedInConnect_2.3

The codes (R scripts) used to process the ecoforestry inventory into impedance rasters are available from the corresponding author upon request.

**REFERENCES**

Ager, A. A., & Clifton, Caty. (2005). *Software for calculating vegetation disturbance and recovery by using the equivalent clearcut area model.* (PNW-GTR-637; p. PNW-GTR-637). U.S. Department of Agriculture, Forest Service, Pacific Northwest Research Station. https://doi.org/10.2737/PNW-GTR-637

Aires, U. R. V., da Silva, D. D., Moreira, M. C., Ribeiro, C. A. A. S., & Ribeiro, C. B. de M. (2020). The Use of the Normalized Difference Vegetation Index to Analyze the Influence of Vegetation Cover Changes on the Streamflow in the Manhuaçu River Basin, Brazil. *Water Resources Management*. https://doi.org/10.1007/s11269-020-02536-1

B.C. Ministry of Forests. (2001). *Watershed Assessment Procedure Guidebook* (p. 47). B.C. Ministry of Forests. http://www.llbc.leg.bc.ca/public/PubDocs/bcdocs/330041/WAPGdbk.pdf

Borselli, L., Cassi, P., & Torri, D. (2008). Prolegomena to sediment and flow connectivity in the landscape: A GIS and field numerical assessment. *CATENA*, *75*(3), 268–277. https://doi.org/10.1016/j.catena.2008.07.006

Boucher, Y., Arseneault, D., Sirois, L., & Blais, L. (2009). Logging pattern and landscape changes over the last century at the boreal and deciduous forest transition in Eastern Canada. *Landscape Ecology*, *24*(2), 171–184. https://doi.org/10.1007/s10980-008-9294-8

Brierley, G., Fryirs, K., & Jain, V. (2006). Landscape connectivity: The geographic basis of geomorphic applications. *Area*, *38*(2), 165–174. https://doi.org/10.1111/j.1475-4762.2006.00671.x

Calsamiglia, A., Fortesa, J., García-Comendador, J., Lucas-Borja, M. E., Calvo-Cases, A., & Estrany, J. (2018). Spatial patterns of sediment connectivity in terraced lands: Anthropogenic

controls of catchment sensitivity. *Land Degradation & Development*, *29*(4), 1198–1210. https://doi.org/10.1002/ldr.2840

Cavalli, M., Trevisani, S., Comiti, F., & Marchi, L. (2013). Geomorphometric assessment of spatial sediment connectivity in small Alpine catchments. *Geomorphology*, *188*, 31–41. https://doi.org/10.1016/j.geomorph.2012.05.007

Cossart, E., Viel, V., Lissak, C., Reulier, R., Fressard, M., & Delahaye, D. (2018). How might sediment connectivity change in space and time? *Land Degradation & Development*, *29*(8), 2595–2613. https://doi.org/10.1002/ldr.3022

Coulthard, T. J., & Van De Wiel, M. J. (2017). Modelling long term basin scale sediment connectivity, driven by spatial land use changes. *Geomorphology*, *277*, 265–281. https://doi.org/10.1016/j.geomorph.2016.05.027

Crema, S., & Cavalli, M. (2018). SedInConnect: A stand-alone, free and open source tool for the assessment of sediment connectivity. *Computers & Geosciences*, *111*, 39–45. https://doi.org/10.1016/j.cageo.2017.10.009

Czuba, J. A., & Foufoula-Georgiou, E. (2015). Dynamic connectivity in a fluvial network for identifying hotspots of geomorphic change. *Water Resources Research*, *51*(3), 1401–1421. https://doi.org/10.1002/2014WR016139

Foerster, S., Wilczok, C., Brosinsky, A., & Segl, K. (2014). Assessment of sediment connectivity from vegetation cover and topography using remotely sensed data in a dryland catchment in the Spanish Pyrenees. *Journal of Soils and Sediments*, *14*(12), 1982–2000. https://doi.org/10.1007/s11368-014-0992-3

Fryirs, K. A. (2017). River sensitivity: A lost foundation concept in fluvial geomorphology. *Earth Surface Processes and Landforms*, *42*(1), 55–70. https://doi.org/10.1002/esp.3940

Gilbert, C. G., & Dutton, C. E. (1880). *Report on the Geology of the Henry Mountains*. US Government Printing Office.

Giles-Hansen, K., Li, Q., & Wei, X. (2019). The Cumulative Effects of Forest Disturbance and Climate Variability on Streamflow in the Deadman River Watershed. *Forests*, *10*(2), 196. https://doi.org/10.3390/f10020196

Goldin, B. (2015). *Geomorphometric analysis and sediment dynamics in mountainous basins: Spatial and temporal scales* [Università degli Studi di Padova]. http://paduaresearch.cab.unipd.it/7772/1/Goldin_Beatrice_tesi.pdf

Grischott, R., Kober, F., Lupker, M., Hippe, K., Ivy-Ochs, S., Hajdas, I., Salcher, B., & Christl, M. (2017). Constant denudation rates in a high alpine catchment for the last 6 kyrs: Alpine $^{10}$Be denudation rates over 6 kyr. *Earth Surface Processes and Landforms*, *42*(7), 1065–1077. https://doi.org/10.1002/esp.4070

Heckmann, T., Cavalli, M., Cerdan, O., Foerster, S., Javaux, M., Lode, E., Smetanová, A., Vericat, D., & Brardinoni, F. (2018). Indices of sediment connectivity: Opportunities, challenges and limitations. *Earth-Science Reviews*, *187*, 77–108. https://doi.org/10.1016/j.earscirev.2018.08.004

Hétu, B., & Gray, J. T. (1980). Évolution postglaciaire des versants de la région de Mont-Louis, Gaspésie, Québec. *Géographie physique et Quaternaire*, *34*(2), 187–208. https://doi.org/10.7202/1000397ar

Hooke, J., & Sandercock, P. (2017). *Combating Desertification and Land Degradation: Spatial Strategies Using Vegetation*. Springer International Publishing. https://doi.org/10.1007/978-3-319-44451-2

Hudson, R. (2000). Snowpack recovery in regenerating coastal British Columbia clearcuts. *Canadian Journal of Forest Research*, *30*(4), 548–556.

Langevin, R., & Plamondon, A. P. (2004). *Méthode de calcul de l'aire équivalente de coupe d'un bassin versant en relation avec le débit de pointe des cours d'eau dans la forêt à dominance résineuse* (p. 20). Ressources naturelles, Faune et Parcs, Québec. https://mffp.gouv.qc.ca/publications/forets/connaissances/methode-calcul.pdf

Li, Q., Wei, X., Zhang, M., Liu, W., Fan, H., Zhou, G., Giles-Hansen, K., Liu, S., & Wang, Y. (2017). Forest cover change and water yield in large forested watersheds: A global synthetic assessment. *Ecohydrology*, *10*(4), e1838. https://doi.org/10.1002/eco.1838

Lisenby, P. E., Fryirs, K. A., & Thompson, C. J. (2019). River sensitivity and sediment connectivity as tools for assessing future geomorphic channel behavior. *International Journal of River Basin Management*, 1–15. https://doi.org/10.1080/15715124.2019.1672705

Lizaga, I., Quijano, L., Palazón, L., Gaspar, L., & Navas, A. (2018). Enhancing Connectivity Index to Assess the Effects of Land Use Changes in a Mediterranean Catchment. *Land Degradation & Development*, *29*(3), 663–675. https://doi.org/10.1002/ldr.2676

Llena, M., Vericat, D., Cavalli, M., Crema, S., & Smith, M. W. (2019). The effects of land use and topographic changes on sediment connectivity in mountain catchments. *Science of The Total Environment*, *660*, 899–912. https://doi.org/10.1016/j.scitotenv.2018.12.479

López-Vicente, M., González-Romero, J., & Lucas-Borja, M. E. (2020). Forest fire effects on sediment connectivity in headwater sub-catchments: Evaluation of indices performance. *Science of The Total Environment*, *732*, 139206. https://doi.org/10.1016/j.scitotenv.2020.139206

López-Vicente, M., Nadal-Romero, E., & Cammeraat, E. L. H. (2017). Hydrological Connectivity Does Change Over 70 Years of Abandonment and Afforestation in the Spanish Pyrenees. *Land Degradation & Development*, *28*(4), 1298–1310. https://doi.org/10.1002/ldr.2531

López-Vicente, M., Poesen, J., Navas, A., & Gaspar, L. (2013). Predicting runoff and sediment connectivity and soil erosion by water for different land use scenarios in the Spanish Pre-Pyrenees. *CATENA*, *102*, 62–73. https://doi.org/10.1016/j.catena.2011.01.001

López-Vicente, Manuel, & Ben-Salem, N. (2019). Computing structural and functional flow and sediment connectivity with a new aggregated index: A case study in a large Mediterranean catchment. *Science of The Total Environment*, *651*, 179–191. https://doi.org/10.1016/j.scitotenv.2018.09.170

Martini, L., Faes, L., Picco, L., Iroumé, A., Lingua, E., Garbarino, M., & Cavalli, M. (2020). Assessing the effect of fire severity on sediment connectivity in central Chile. *Science of The Total Environment*, *728*, 139006. https://doi.org/10.1016/j.scitotenv.2020.139006

MFFP. (2018). *Cartographie du 5e inventaire écoforestier du Québec méridional: Méthodes et données associées* (p. 111). Ministère des Forêts, de la Faune et des Parcs (MFFP). http://collections.banq.qc.ca/ark:/52327/3466439

Moreno-de-las-Heras, M., Merino-Martín, L., Saco, P. M., Espigares, T., Gallart, F., & Nicolau, J. M. (2020). Structural and functional control of surface-patch to hillslope-scale runoff and sediment connectivity in Mediterranean-dry reclaimed slope systems. *Hydrology and Earth System Sciences*. https://doi.org/10.5194/hess-2019-572

MTES. (2020). *Registraire des entreprises*. Ministère du travail, de l'emploi et de la solidarité sociale. http://www.registreentreprises.gouv.qc.ca/fr/default.aspx

Nicoll, T., & Brierley, G. (2017). Within-catchment variability in landscape connectivity measures in the Garang catchment, upper Yellow River. *Geomorphology*, *277*, 197–209. https://doi.org/10.1016/j.geomorph.2016.03.014

Ning, D., Zhang, M., Ren, S., Hou, Y., Yu, L., & Meng, Z. (2017). Predicting hydrological response to forest changes by simple statistical models: The selection of the best indicator of

forest changes with a hydrological perspective. *IOP Conference Series: Earth and Environmental Science*, *52*, 012059. https://doi.org/10.1088/1742-6596/52/1/012059

Ortíz-Rodríguez, A. J., Muñoz-Robles, C., & Borselli, L. (2019). Changes in connectivity and hydrological efficiency following wildland fires in Sierra Madre Oriental, Mexico. *Science of The Total Environment*, *655*, 112–128. https://doi.org/10.1016/j.scitotenv.2018.11.236

Pelletier, T. S. (2014). *Vivre et pêcher dans les Notre-Dame. Excursion archéologique sur le barachois de Mont-Louis au Régime français.* (Les Presses de l'Université Laval).

Persichillo, M. G., Bordoni, M., Cavalli, M., Crema, S., & Meisina, C. (2018). The role of human activities on sediment connectivity of shallow landslides. *CATENA*, *160*, 261–274. https://doi.org/10.1016/j.catena.2017.09.025

Pike, R. G., Redding, T. E., Wilford, D. J., Reiter, M. L., & Toews, D. A. A. (2010). Detecting and Predicting Changes in Watersheds. In *Compendium of forest hydrology and geomorphology in British Columbia.* (B.C. Min. For. Range, For. Sci. Prog., Victoria, B.C. and FORREX Forum for Research and Extension in Natural Resources, p. 26). B.C. Land Manag. Handb. www.for.gov.bc.ca/hfd/pubs/Docs/Lmh/Lmh66.htm

Pinna, S., Malenfant, A., Hébert, B., Côté, M., Biondo, S., & Consortium en foresterie Gaspésie-Les-Îles. (2009). *Portrait forestier historique de la Gaspésie*. http://collections.banq.qc.ca/ark:/52327/bs2011322

Plamondon, A. P. (2004). *La récolte forestière et les débits de pointe: État des connaissances sur la prévision des augmentations des pointes, le concept de l'aire équivalente de coupe acceptable et les taux régressifs des effets de la coupe sur les débits de pointe* (p. 236). Ressources naturelles, Faune et Parcs, Québec.

673 Poeppl, R. E., Keesstra, S. D., & Maroulis, J. (2017). A conceptual connectivity framework for
674 understanding geomorphic change in human-impacted fluvial systems. *Geomorphology*,
675 *277*, 237–250. https://doi.org/10.1016/j.geomorph.2016.07.033
676 Prosdocimi, M., Burguet, M., Di Prima, S., Sofia, G., Terol, E., Rodrigo Comino, J., Cerdà, A., &
677 Tarolli, P. (2017). Rainfall simulation and Structure-from-Motion photogrammetry for
678 the analysis of soil water erosion in Mediterranean vineyards. *Science of The Total*
679 *Environment*, *574*, 204–215. https://doi.org/10.1016/j.scitotenv.2016.09.036
680 Renard, K. G. (1997). *Predicting soil erosion by water: A guide to conservation planning with the*
681 *Revised Universal Soil Loss Equation (RUSLE)*. United States Government Printing.
682 Schopper, N., Mergili, M., Frigerio, S., Cavalli, M., & Poeppl, R. (2019). Analysis of lateral
683 sediment connectivity and its connection to debris flow intensity patterns at different
684 return periods in the Fella River system in northeastern Italy. *Science of The Total*
685 *Environment*, *658*, 1586–1600. https://doi.org/10.1016/j.scitotenv.2018.12.288
686 Talbot, J., & Plamondon, A. P. (2002). The Diminution of Snowmelt Rate with Forest Regrowth as
687 an Index of Peak Flow Hydrologic Recovery, Montmorency Forest, Quebec. *Proceedings*
688 *of the 59th Eastern Snow Conference*, 7.
689 Talbot, J., Plamondon, A. P., Lévesque, D., Aubé, D., Prévos, M., Chazalmartin, F., & Gnocchini,
690 M. (2006). Relating snow dynamics and balsam fir stand characteristics, Montmorency
691 Forest, Quebec. *Hydrological Processes*, *20*(5), 1187–1199.
692 https://doi.org/10.1002/hyp.5938
693 Trevisani, S., & Cavalli, M. (2016). Topography-based flow-directional roughness: Potential and
694 challenges. *Earth Surface Dynamics*, *4*(2), 343–358. https://doi.org/10.5194/esurf-4-
695 343-2016

Wainwright, J., Turnbull, L., Ibrahim, T. G., Lexartza-Artza, I., Thornton, S. F., & Brazier, R. E. (2011). Linking environmental régimes, space and time: Interpretations of structural and functional connectivity. *Geomorphology*, *126*(3–4), 387–404. https://doi.org/10.1016/j.geomorph.2010.07.027

Wei, X., Li, Q., Zhang, M., Liu, W., & Fan, H. (2016). Forest cover changes and hydrology in large watersheds. In *Forest hydrology: Processes, management and assessment* (pp. 180–191). CAB International.

Wei, X., & Zhang, M. (2011). *Research Methods for Assessing the Impacts of Forest Disturbance on Hydrology at Large-scale Watersheds* (Landscape Ecology in Forest Management and Conservation, p. 29). Springer Berlin Heidelberg.

Winkler, R., Boon, S., & Hill, C. (2017). Equivalent Clearcut Area as an Indicator of Hydrologic Change in Snow-dominated Watersheds of Southern British Columbia. *Prov. B.C., Extension Note*, 10.

Wischmeier, W. H., & Smith, D. D. (1978). *Predicting rainfall erosion losses: A guide to conservation planning* (Issue 537). Department of Agriculture, Science and Education Administration.

Wohl, E. (2017). Connectivity in rivers. *Progress in Physical Geography: Earth and Environment*, *41*(3), 345–362. https://doi.org/10.1177/0309133317714972

Wohl, E., Brierley, G., Cadol, D., Coulthard, T. J., Covino, T., Fryirs, K. A., Grant, G., Hilton, R. G., Lane, S. N., Magilligan, F. J., Meitzen, K. M., Passalacqua, P., Poeppl, R. E., Rathburn, S. L., & Sklar, L. S. (2019). Connectivity as an emergent property of geomorphic systems: Geomorphic connectivity. *Earth Surface Processes and Landforms*, *44*(1), 4–26. https://doi.org/10.1002/esp.4434

Zanandrea, F., Michel, G. P., & Kobiyama, M. (2020). Impedance influence on the index of sediment connectivity in a forested mountainous catchment. *Geomorphology*, *351*, 106962. https://doi.org/10.1016/j.geomorph.2019.106962

Zhang, M., Liu, N., Harper, R., Li, Q., Liu, K., Wei, X., Ning, D., Hou, Y., & Liu, S. (2017). A global review on hydrological responses to forest change across multiple spatial scales: Importance of scale, climate, forest type and hydrological regime. *Journal of Hydrology*, *546*, 44–59. https://doi.org/10.1016/j.jhydrol.2016.12.040

Zhang, M., Wei, X., & Li, Q. (2016). A quantitative assessment on the response of flow regimes to cumulative forest disturbances in large snow-dominated watersheds in the interior of British Columbia, Canada: The Response of Flow Regimes, Cumulative Forest Disturbances, Large Snow-Dominated Watersheds. *Ecohydrology*, *9*(5), 843–859. https://doi.org/10.1002/eco.1687

Zhang, M., Wei, X., Sun, P., & Liu, S. (2012). The effect of forest harvesting and climatic variability on runoff in a large watershed: The case study in the Upper Minjiang River of Yangtze River basin. *Journal of Hydrology*, *464–465*, 1–11. https://doi.org/10.1016/j.jhydrol.2012.05.050

**Table 1: Recent studies assessing the evolution of hydrosedimentary connectivity induced by land use/vegetation cover change, using IC (Cavalli et al., 2013).**

| Year | Author | Environmental context | Change type | Impedance method | Period (yr) | Temporality | Key findings |
|---|---|---|---|---|---|---|---|
| 2014 | Foerster et al. | Mediterranean mountainous (Spain) | Seasonal vegetation change | C-factor (continuous) | <1 | 2 dates | Connectivity depends on the spatial distribution of vegetation |
| 2017 | Lopez-Vicente et al. | Mediterranean mountainous (Spain) | Cultures turned to forest | C-factor (14 classes) | 67 | 6 dates | -Changes in connectivity mainly depends on the changes in vegetation<br>-Afforestation promotes lower and more stable connectivity |
| 2018 | Persichillio et al. | Mediterranean semi-mountainous (Italy) | Agricultural practices | Derived Manning's n (7 classes) | 58 | 5 dates | Vegetation dynamics influences connectivity in a non-linear way |
| 2018 | Martinez-Murillo et al. | Mediterranean mountainous (Spain) | Wildfires, salvage logging | C-factor, Normalized Burn Ratio and vegetation recovery | 4 | 6 dates Pre/post fire | -Wildfires increases connectivity<br>-Connectivity decreases with vegetation recovery |
| 2018 | Lizaga et al. | Mediterranean semi-mountainous (Spain) | Natural afforestation | C-factor (5 classes), total aerial biomass and roughness | 53 | 2 dates | Agricultural lands abandonment decreases connectivity |
| 2019 | Ortiz-Rodriguez et al. | Semi-arid mountainous (Mexico) | Wildfires | Land use mapping (6 classes) and fire severity based on NDVI (3 levels) | <1 | 2 dates Pre/post fire | Wildfires significantly increases connectivity |
| 2019 | Llena et al. | Mediterranean mountainous (Spain) | Natural afforestation | Derived Manning's n (3 classes) | 53 | 2 dates | Land cover changes directly affects impedance to water and sediment connectivity |
| **2020** | **this study** | **Snow-dominated mountainous (Canada)** | **Anthropic and natural forest disturbances** | **Derived hydrological recovery rates (21 classes)** | **38** | **38 dates** | Connectivity dynamic strongly depends on forest disturbances location<br>Connectivity is highly variable in time |

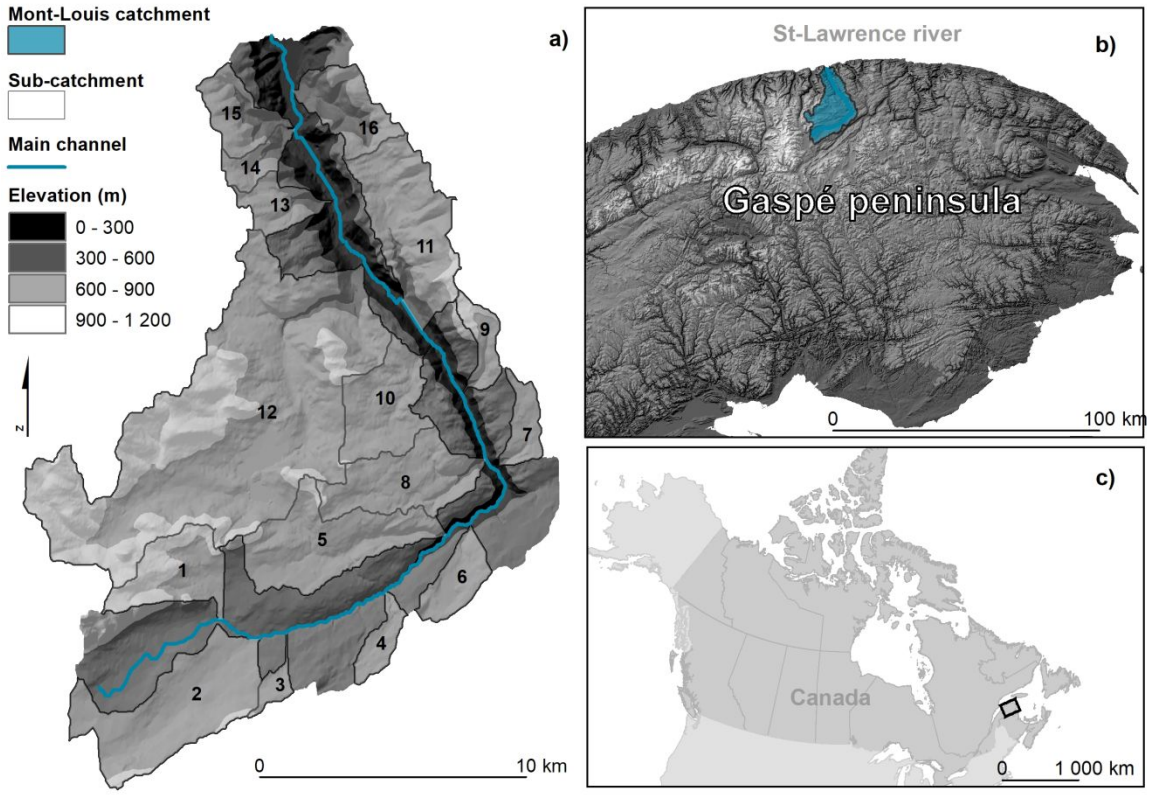


*Figure 1. Mont-Louis catchment location. a) Mont-Louis topographic map and sub-catchments. b) Gaspé peninsula and Mont-Louis catchment location. c) Gaspé peninsula location in Canada.*

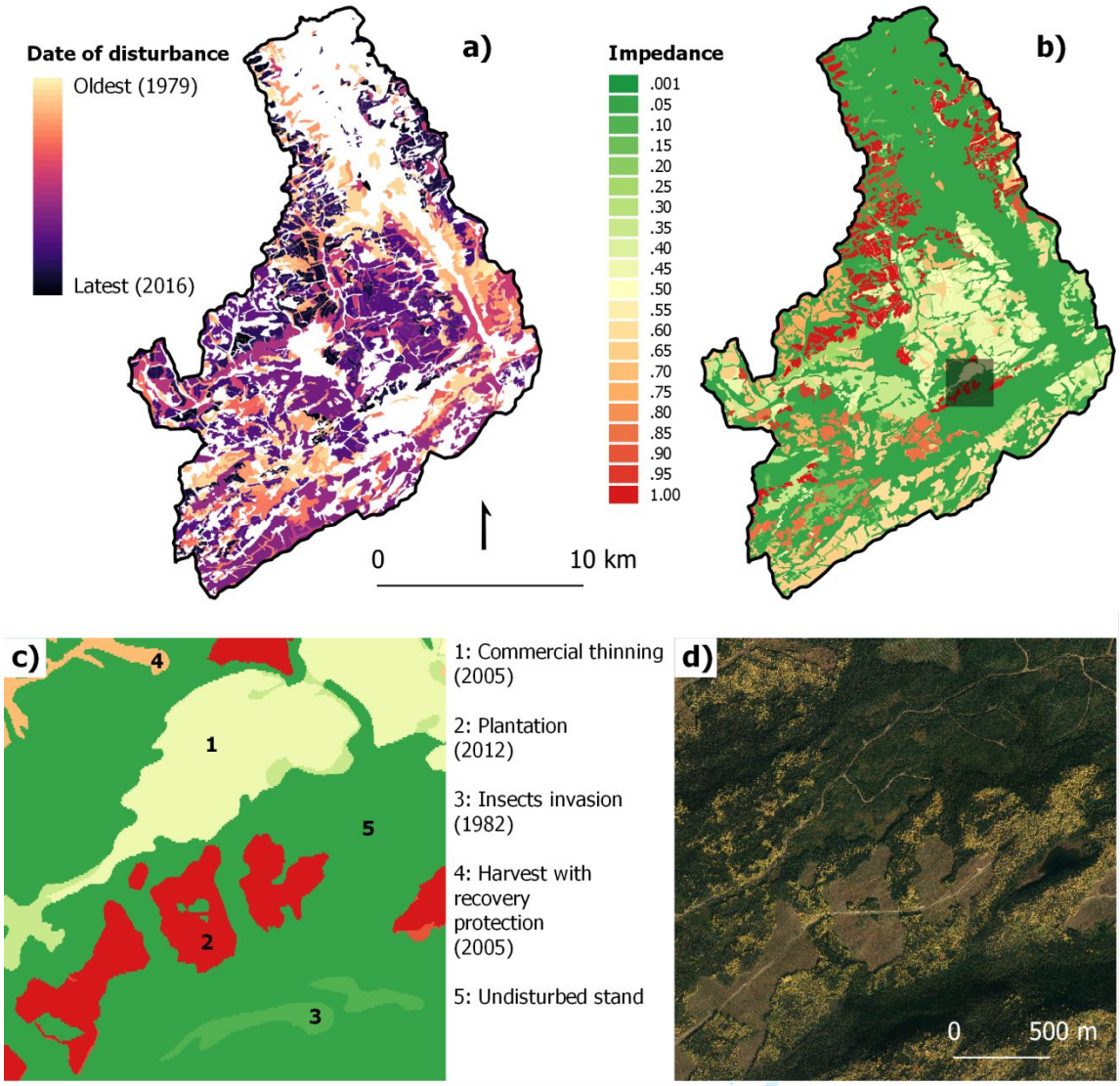


*Figure 2: Processing of the spatiotemporal ecoforestry database. a) Example of the 2016 forest disturbance map (FDM) resulting in the b) 2016 impedance raster ($W_{HR}$), with a zoom-in illustrating c) the high spatial resolution of $W_{HR}$, which depends on the different types of disturbances (1-5), and d) the associated orthophoto (2016).*

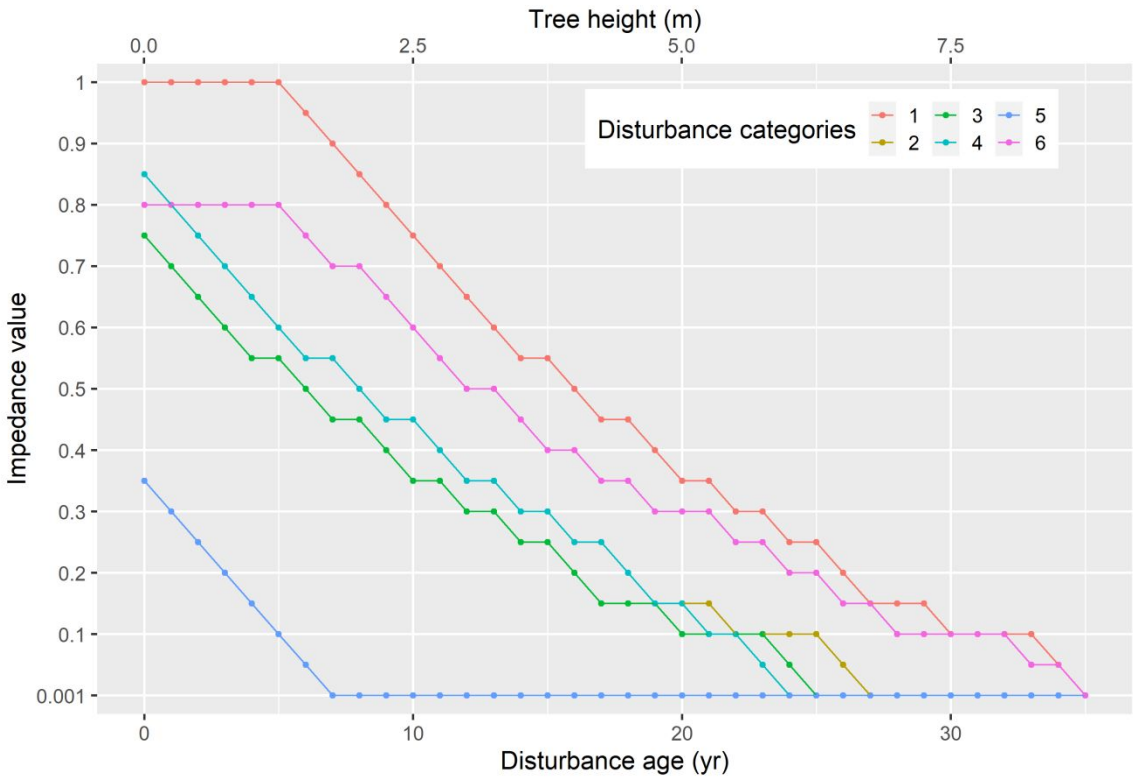


*Figure 3: Temporal evolution of the impedance ($W_{HR}$) used in this study, depending on disturbance age, category and tree height. Values of impedance are directly derived from the snow augmentation coefficient rate (SAC) established by Langevin and Plamondon (2004).*

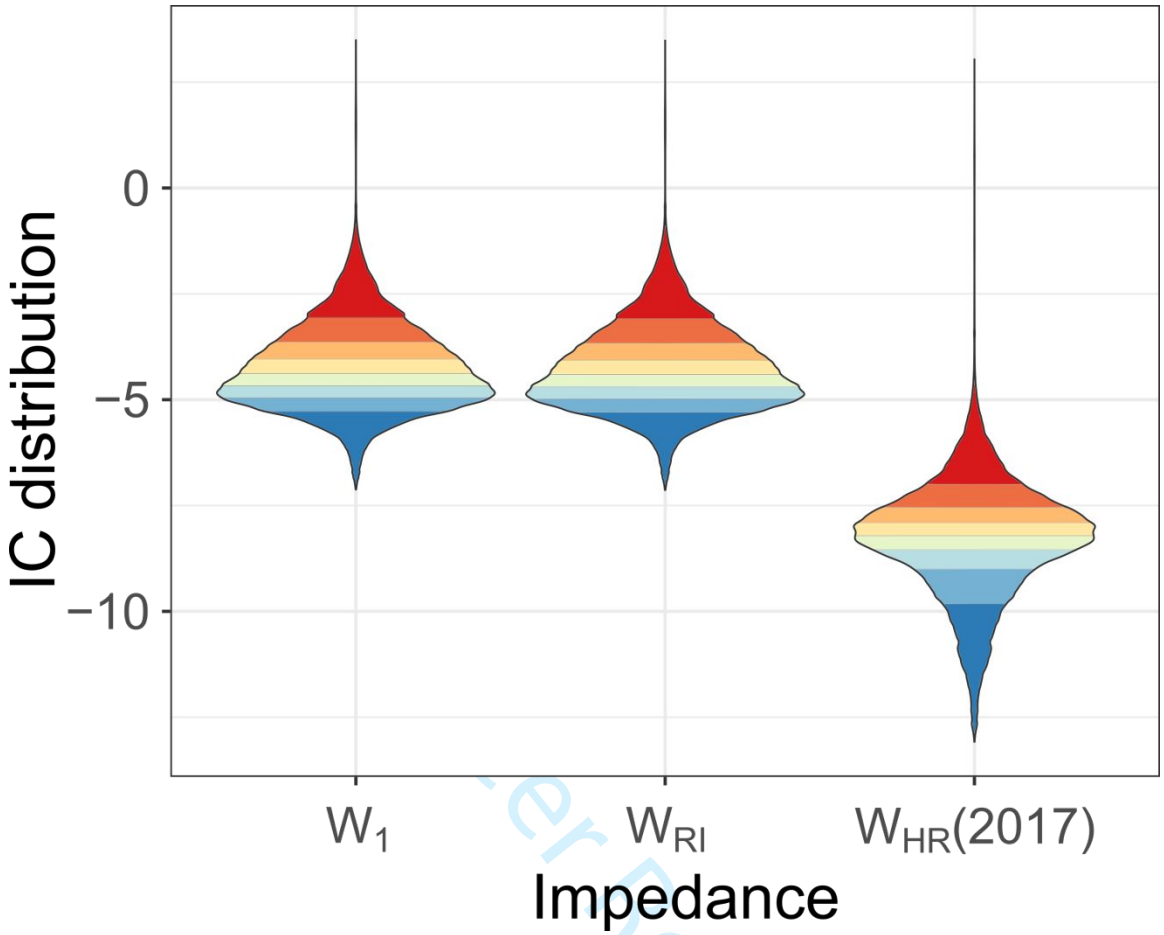


*Figure 4: Violin boxplots of IC values over the Mont-Louis catchment, computed with three impedances ($W_1$, $W_{RI}$, $W_{HR}(2017)$).*

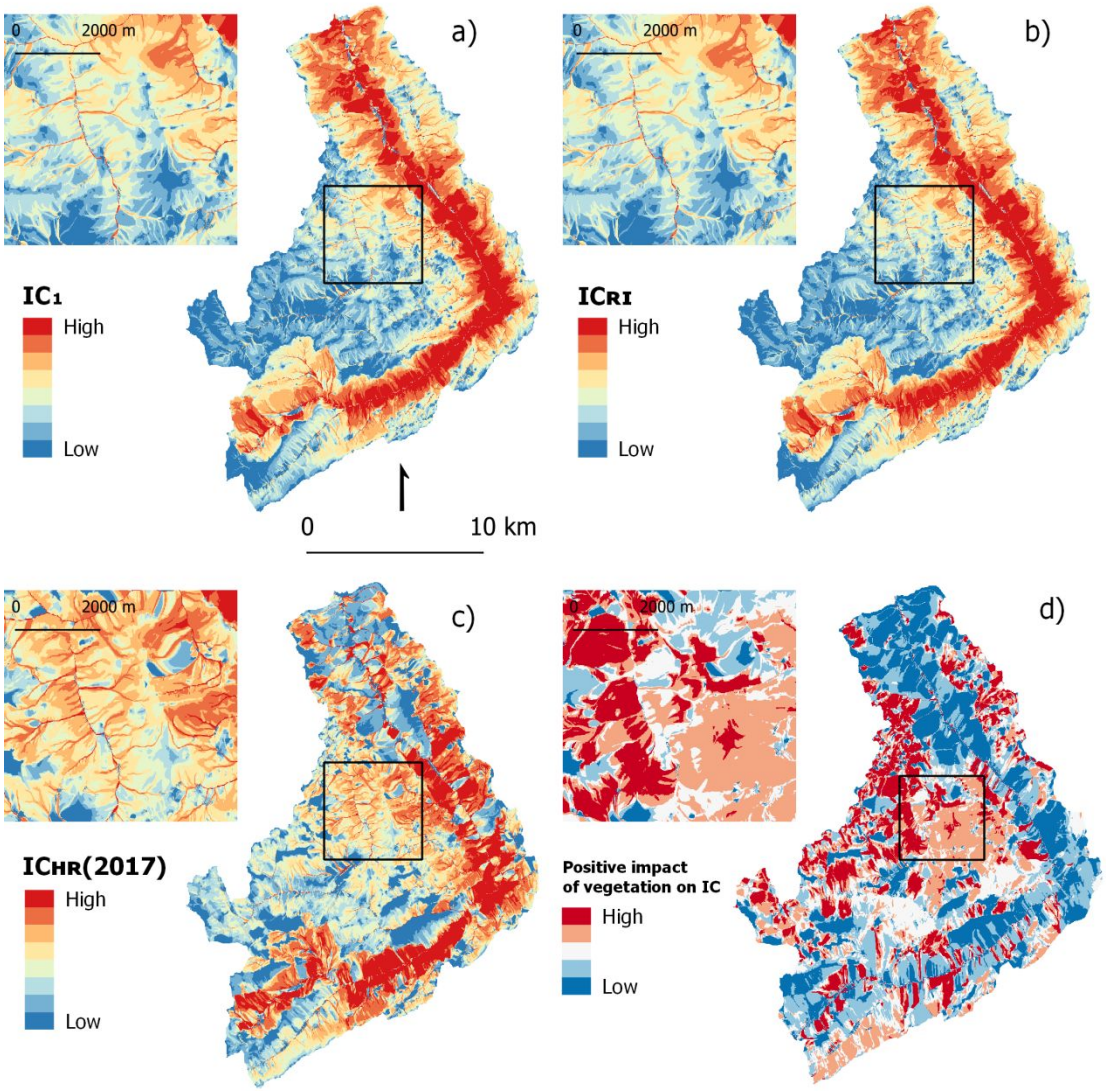


*Figure 5: IC maps depending on the impedance. a) Uniform impedance ($W_1$). b) Topography-based impedance ($W_{RI}$). c) Vegetation-based impedance ($W_{HR}(2017)$). d) Absolute difference between $IC_{HR}(2017)$ and $IC_{RI}$.*

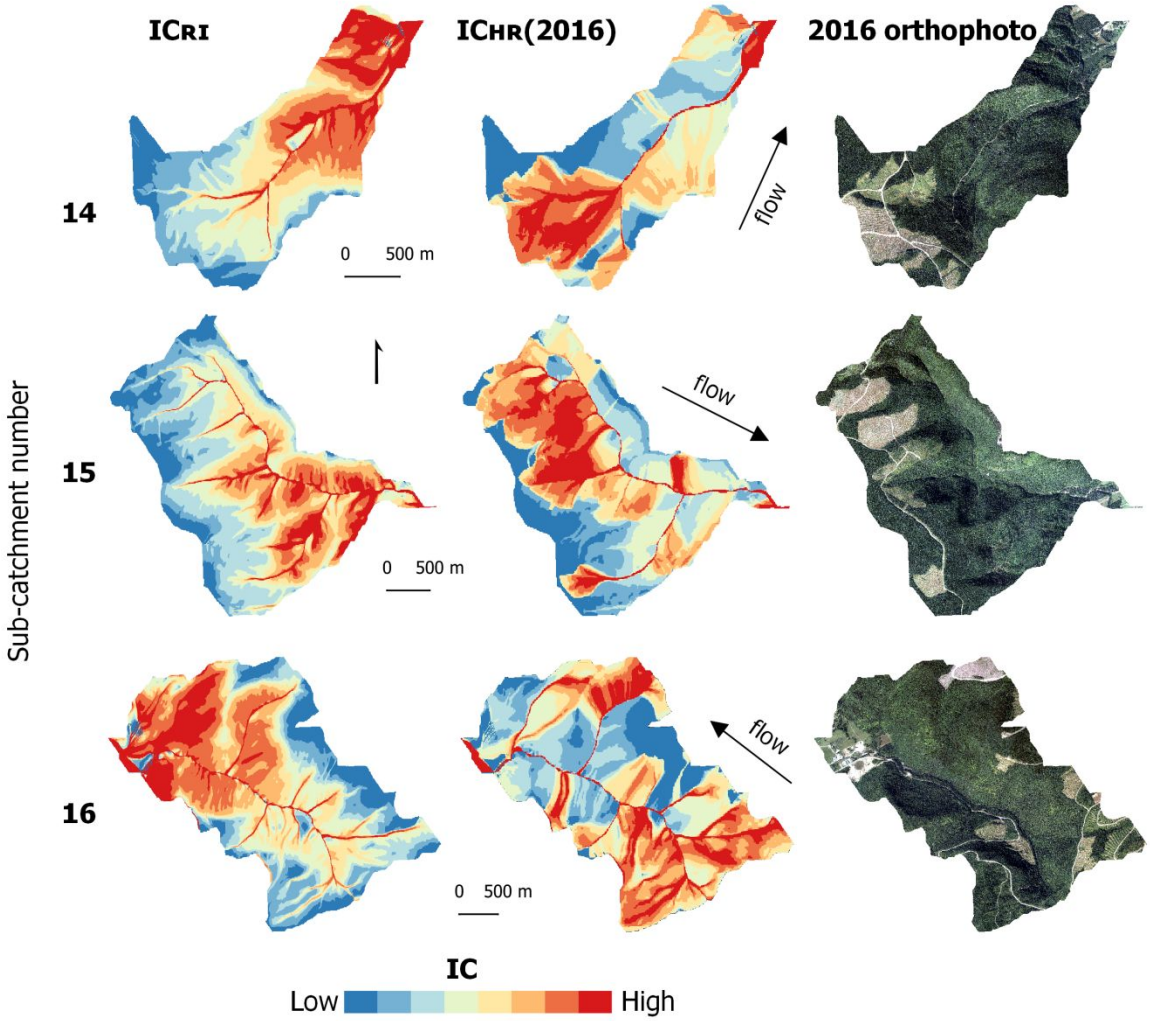


*Figure 6: Comparison of IC in three sub-catchments (14,15,16) when computed with $W_{RI}$ and $W_{HR}$(2016). The 2016 orthophoto reflects the importance of considering the presence (absence) of vegetation.*

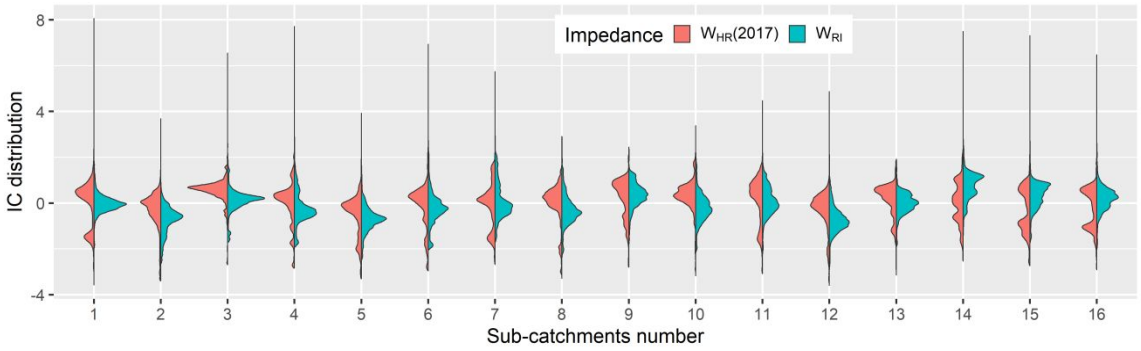


*Figure 7: Distribution of standardized IC values depending on the impedance ($W_{HR}$ and $W_{RI}$), extracted from each sub-catchment.*

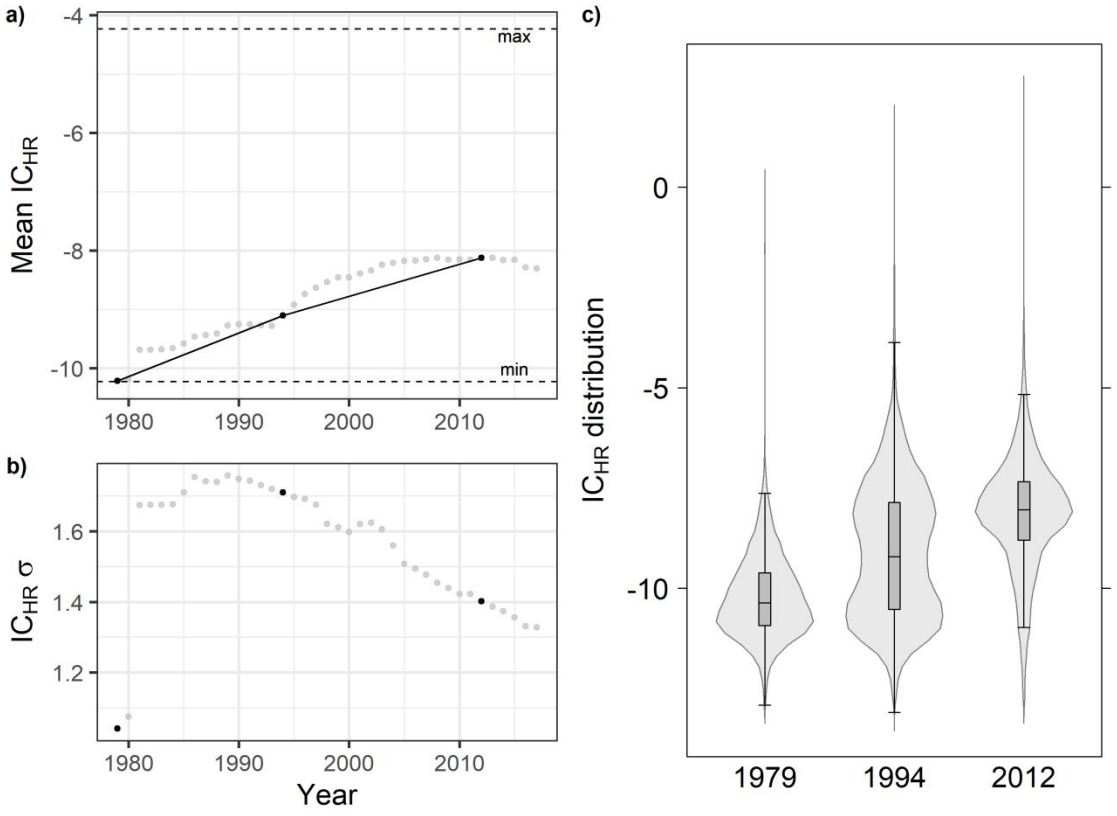


*Figure 8: Temporal evolution of IC over Mont-Louis catchment, from 1979 to 2017. a) Mean value of $IC_{HR}$. Black dashed lines corresponds to the theoretical maximum and minimum possible value of the mean $IC_{HR}$. b) Standard deviation of $IC_{HR}$. c) $IC_{HR}$ distributions for year 1979, 1994 and 2012.*

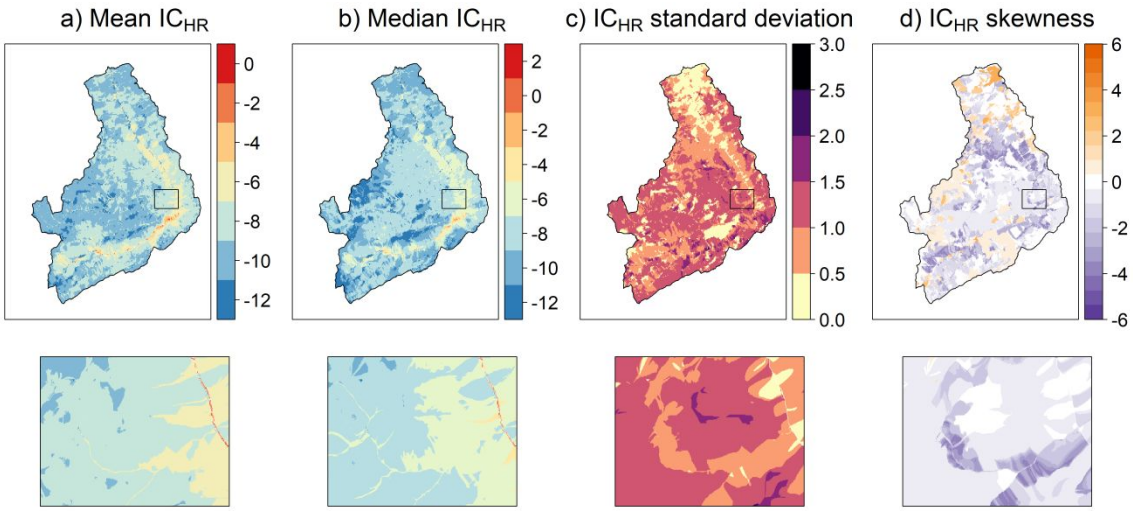


*Figure 9: Spatiotemporal trends over the time-series of IC$_{HR}$ from 1979 to 2017. a) Mean IC$_{HR}$. b) Median IC$_{HR}$. c) IC$_{HR}$ standard deviation. d) IC$_{HR}$ skewness.*

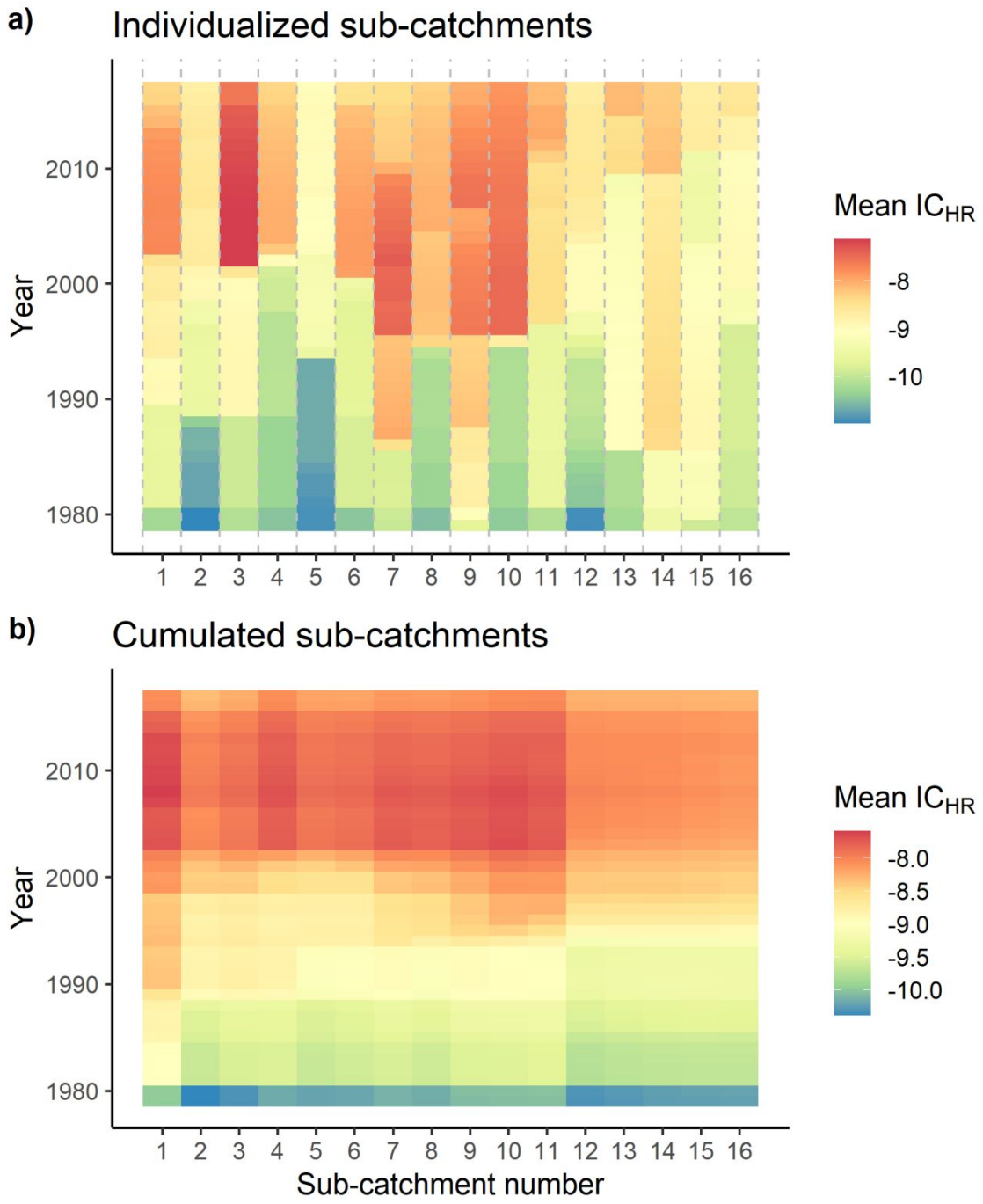


*Figure 10: Spatiotemporal matrix of mean $IC_{HR}$ computed per a) individualized and b) cumulated sub-catchments.*

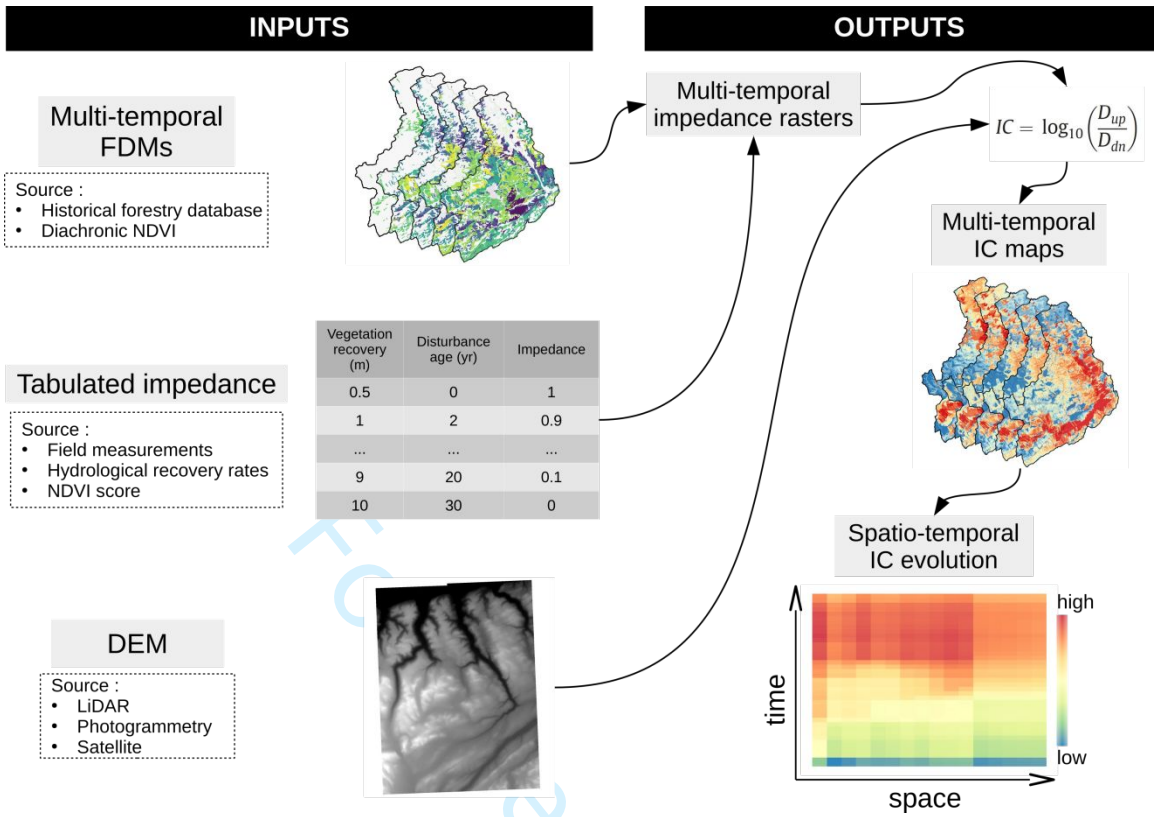


*Figure 11: Synthetic workflow used to assess the interannual evolution of IC using FDMs, tabulated impedances and a DEM.*

**Figure Caption**

Figure 1. Mont-Louis catchment location. a) Mont-Louis topographic map and sub-catchments. b) Gaspé peninsula and Mont-Louis catchment location. c) Gaspé peninsula location in Canada.

Figure 2: Processing of the spatiotemporal ecoforestry database. a) Example of the 2016 forest disturbance map (FDM) resulting in the b) 2016 impedance raster ($W_{HR}$), with a zoom-in illustrating c) the high spatial resolution of $W_{HR}$, which depends on the different types of disturbances (1-5), and d) the associated orthophoto (2016).

Figure 3: Temporal evolution of the impedance ($W_{HR}$) used in this study, depending on disturbance age, category and tree height. Values of impedance are directly derived from the snow augmentation coefficient rate (SAC) established by Langevin and Plamondon (2004).

Figure 4: Violin boxplots of IC values over the Mont-Louis catchment, computed with three impedances ($W_1$, $W_{RI}$, $W_{HR}$(2017)).

Figure 5: IC maps depending on the impedance. a) Uniform impedance ($W_1$). b) Topography-based impedance ($W_{RI}$). c) Vegetation-based impedance ($W_{HR}$(2017)). d) Absolute difference between $IC_{HR}$(2017) and $IC_{RI}$.

Figure 6: Comparison of IC in three sub-catchments (14,15,16) when computed with $W_{RI}$ and $W_{HR}$(2016). The 2016 orthophoto reflects the importance of considering the presence (absence) of vegetation.

Figure 7: Distribution of standardized IC values depending on the impedance ($W_{HR}$ and $W_{RI}$), extracted from each sub-catchment.

Figure 8: Temporal evolution of IC over Mont-Louis catchment, from 1979 to 2017. a) Mean value of $IC_{HR}$. Black dashed lines corresponds to the theoretical maximum and minimum possible value of the mean $IC_{HR}$. b) Standard deviation of $IC_{HR}$. c) $IC_{HR}$ distributions for year 1979, 1994 and 2012.

Figure 9: Spatiotemporal trends over the time-series of $IC_{HR}$ from 1979 to 2017. a) Mean $IC_{HR}$. b) Median $IC_{HR}$. c) $IC_{HR}$ standard deviation. d) $IC_{HR}$ skewness.

Figure 10: Spatiotemporal matrix of mean $IC_{HR}$ computed per a) individualized and b) cumulated sub-catchments.

Figure 11: Synthetic workflow used to assess the interannual evolution of IC using FDMs, tabulated impedances and a DEM.

**SUPPLEMENTARY MATERIAL**

**Inter-annual evolution of hydrosedimentary connectivity induced by forest cover change in Mont-Louis catchment**

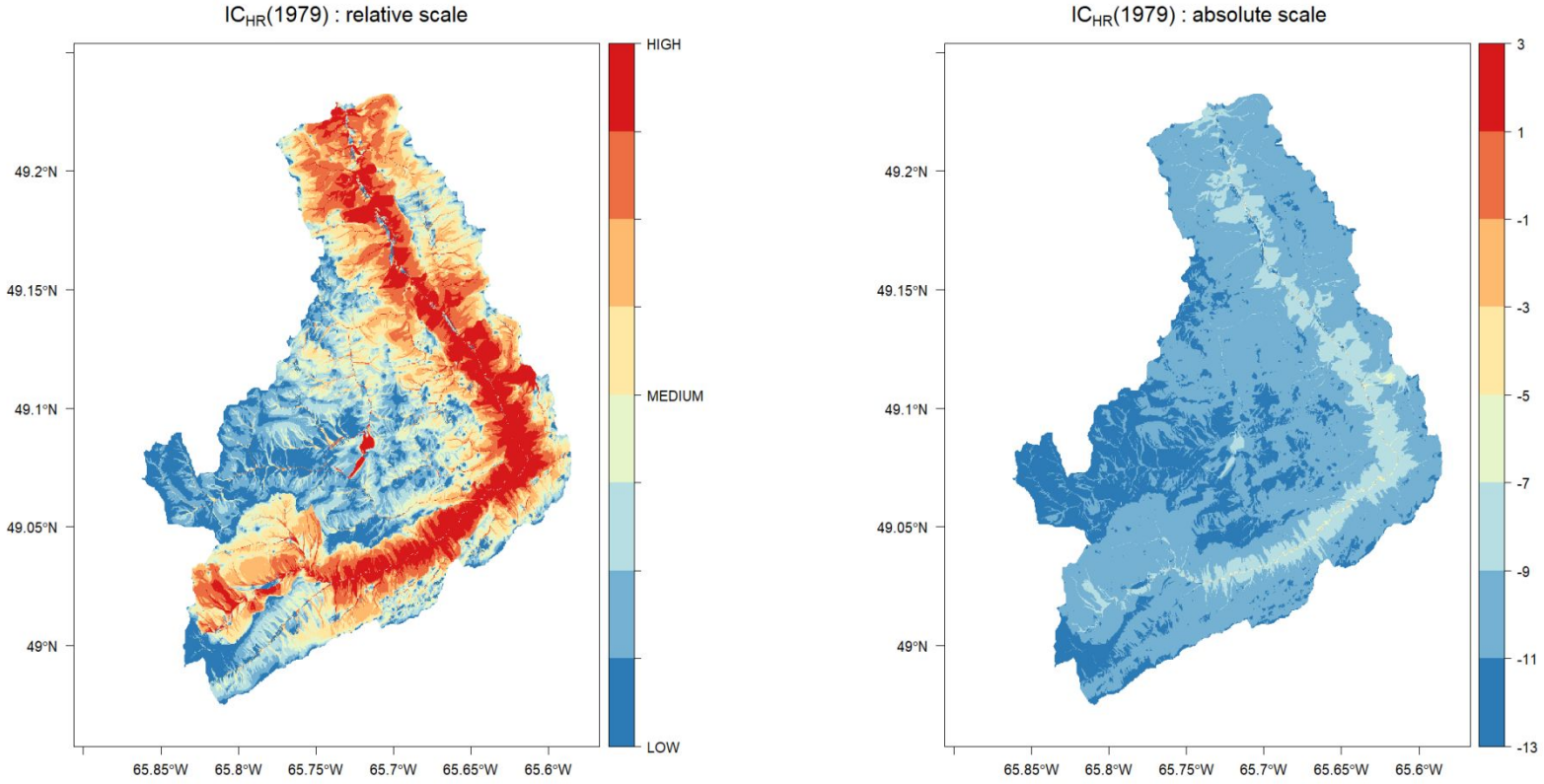


This animation corresponds to the entire time-series of $IC_{HR}$ maps produced in this study, with two different scales. It thus represents the interannual evolution of hydrosedimentary connectivity induced by forest cover change in the Mont-Louis catchment.

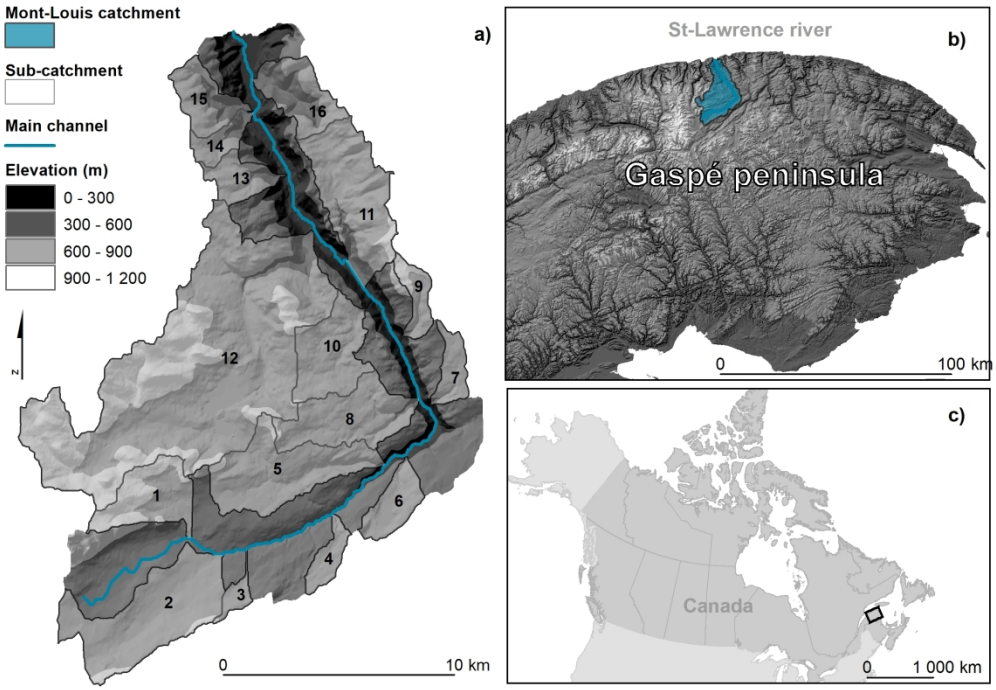


Mont-Louis catchment location. a) Mont-Louis topographic map and sub-catchments. b) Gaspé peninsula and Mont-Louis catchment location. c) Gaspé peninsula location in Canada.

215x150mm (300 x 300 DPI)

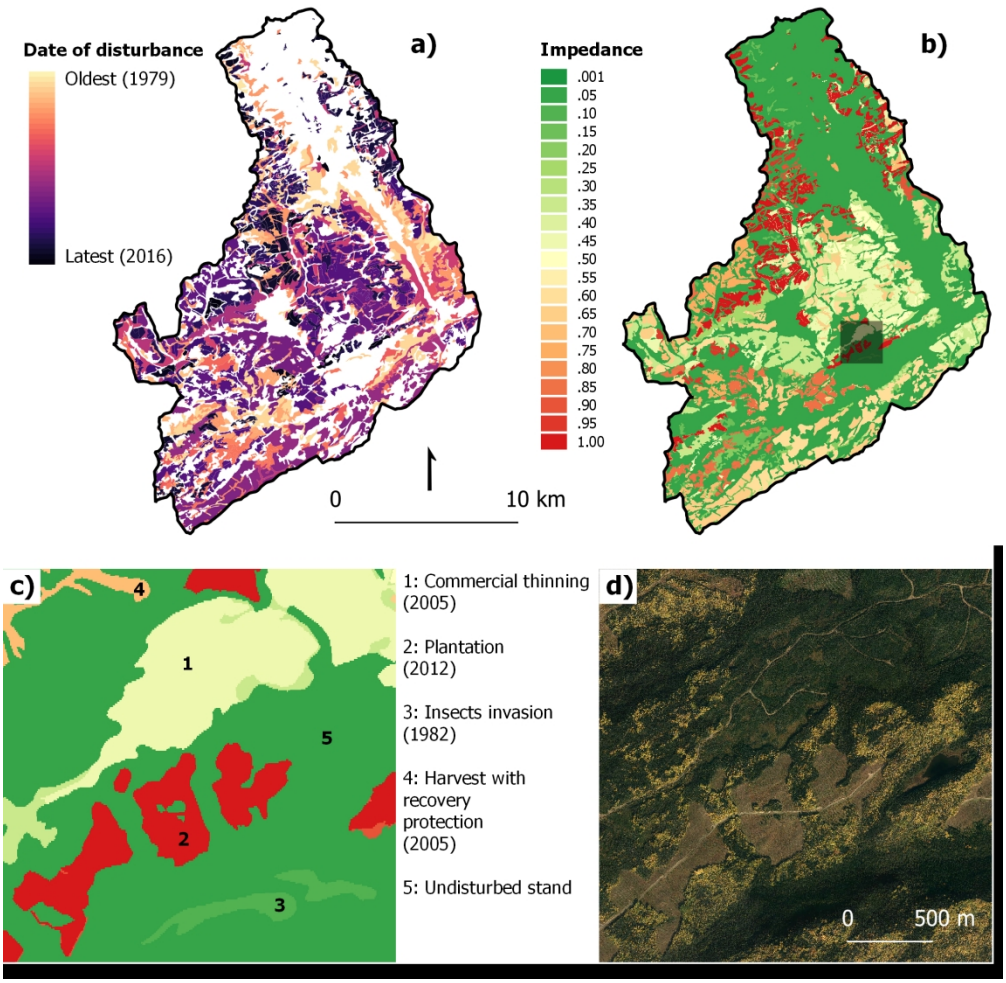


Processing of the spatiotemporal ecoforestry database. a) Example of the 2016 forest disturbance map (FDM) resulting in the b) 2016 impedance raster ($W_{HR}$), with a zoom-in illustrating c) the high spatial resolution of $W_{HR}$, which depends on the different types of disturbances (1-5), and d) the associated orthophoto (2016).

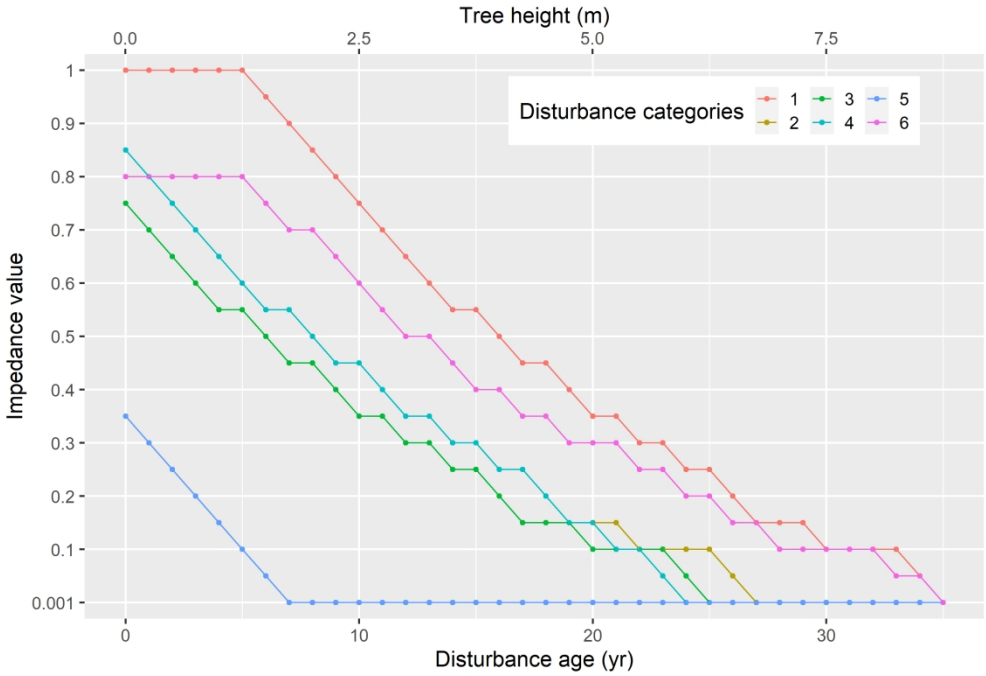


Temporal evolution of the impedance ($W_{HR}$) used in this study, depending on disturbance age, category and tree height. Values of impedance are directly derived from the snow augmentation coefficient rate (SAC) established by Langevin and Plamondon (2004).

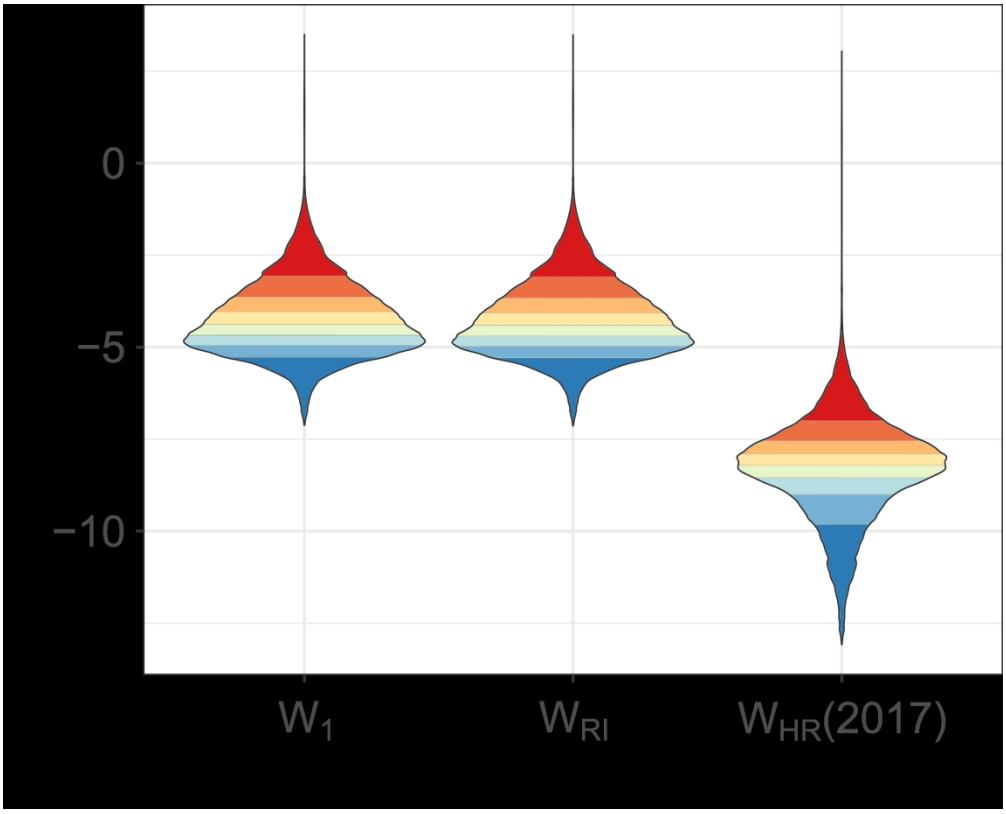


Violin boxplots of IC values over the Mont-Louis catchment, computed with three impedances ($W_1$, $W_{RI}$, $W_{HR}(2017)$).

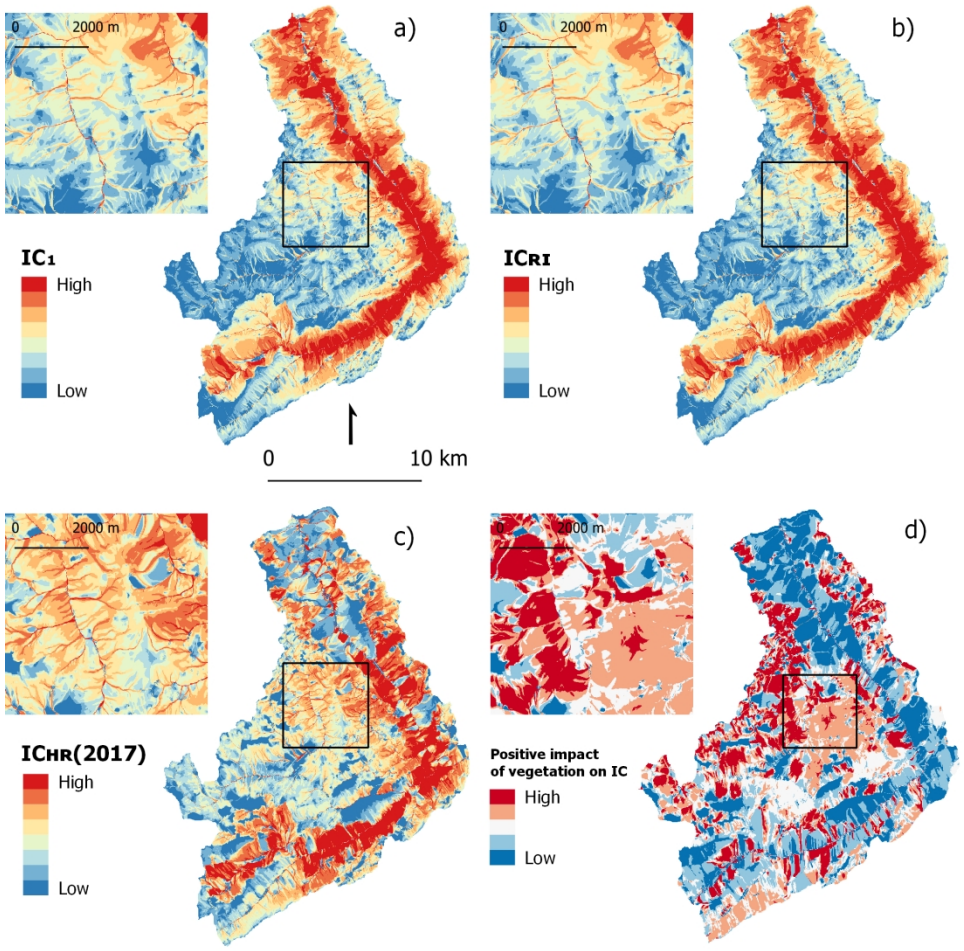


IC maps depending on the impedance. a) Uniform impedance ($W_1$); b) Topography-based impedance ($W_{RI}$); c) Vegetation-based impedance ($W_{HR}(2017)$); d) Absolute difference between $IC_{HR}(2017)$ and $IC_{RI}$.

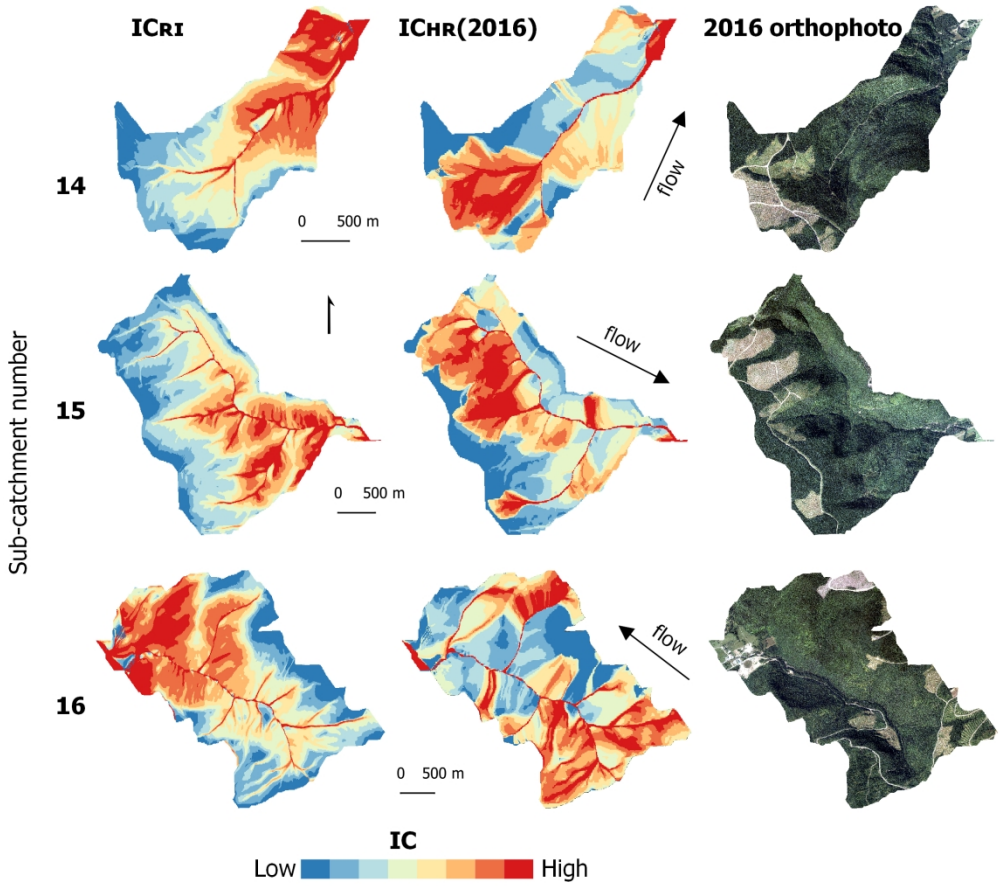


Comparison of IC in three sub-catchments (14,15,16) when computed with $W_{RI}$ and $W_{HR}$(2016). The 2016 orthophoto reflects the importance of considering the presence (absence) of vegetation.

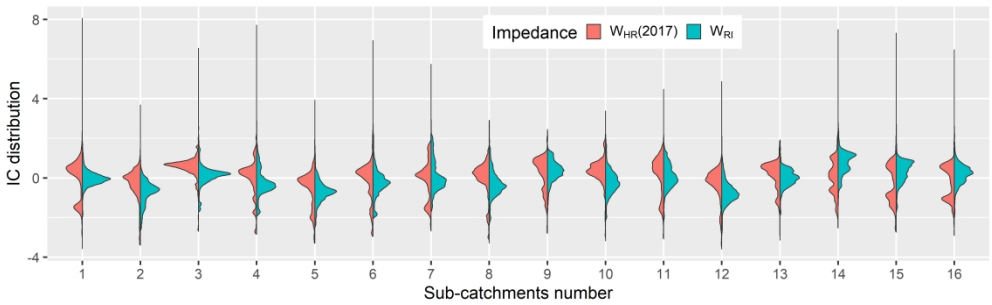


Distribution of standardized IC values depending on the impedance ($W_{HR}$ and $W_{RI}$) and extracted from each sub-catchment.

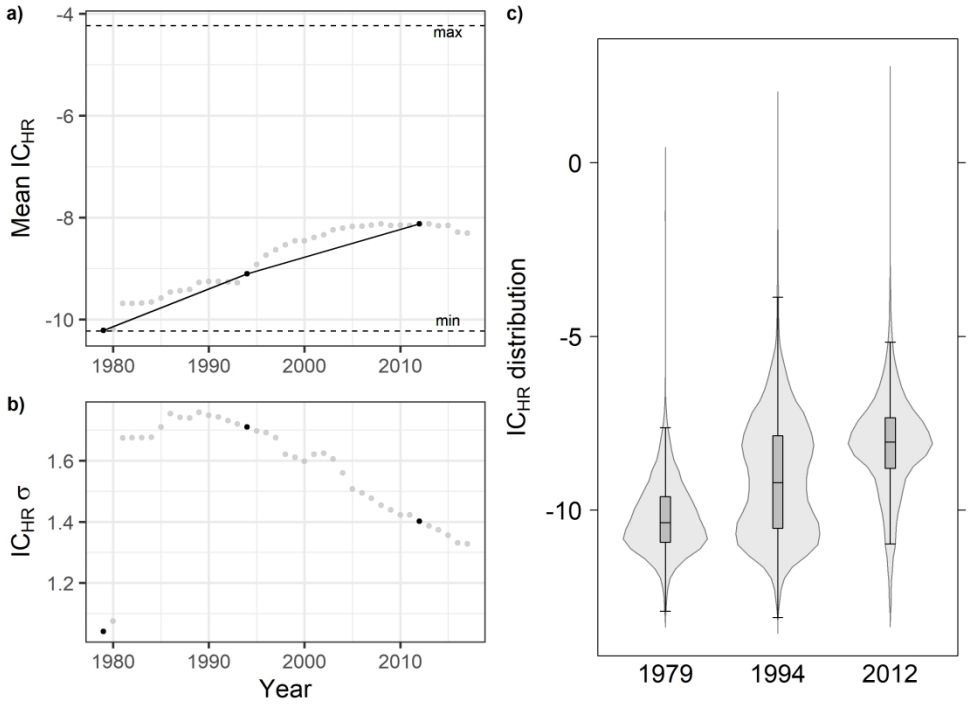


Temporal evolution of IC over the Mont-Louis catchment from 1979 to 2017. a) Mean value of $IC_{HR}$; the black dashed lines correspond to the theoretical minimum and maximum mean $IC_{HR}$ values. b) Standard deviation of $IC_{HR}$. c) $IC_{HR}$ distributions for 1979, 1994, and 2012.

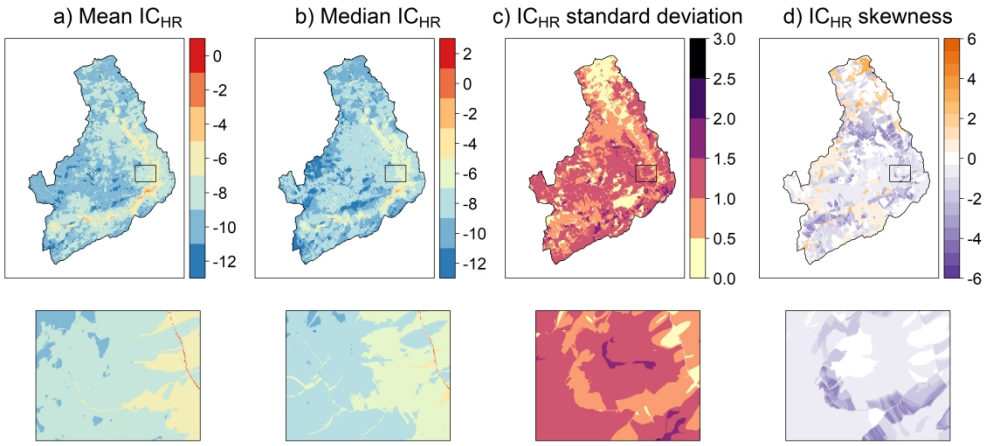


Spatiotemporal trends over the $IC_{HR}$ time-series from 1979 to 2017. a) Mean $IC_{HR}$; b) Median $IC_{HR}$; c) $IC_{HR}$ standard deviation; d) $IC_{HR}$ skewness. The insets show details of the area indicated on the catchment map.

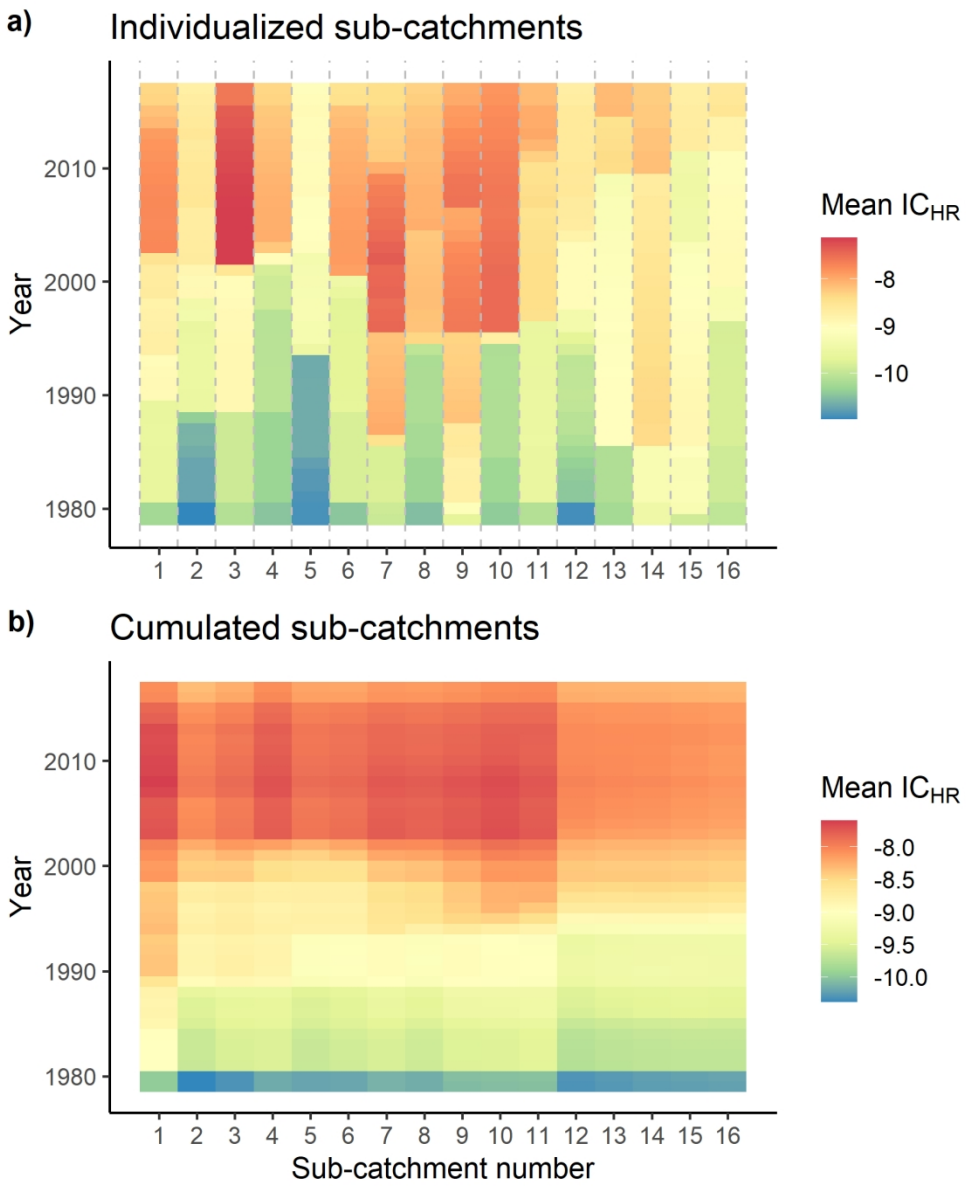


Spatiotemporal matrix of mean $IC_{HR}$ computed per a) individualized and b) cumulated sub-catchments.

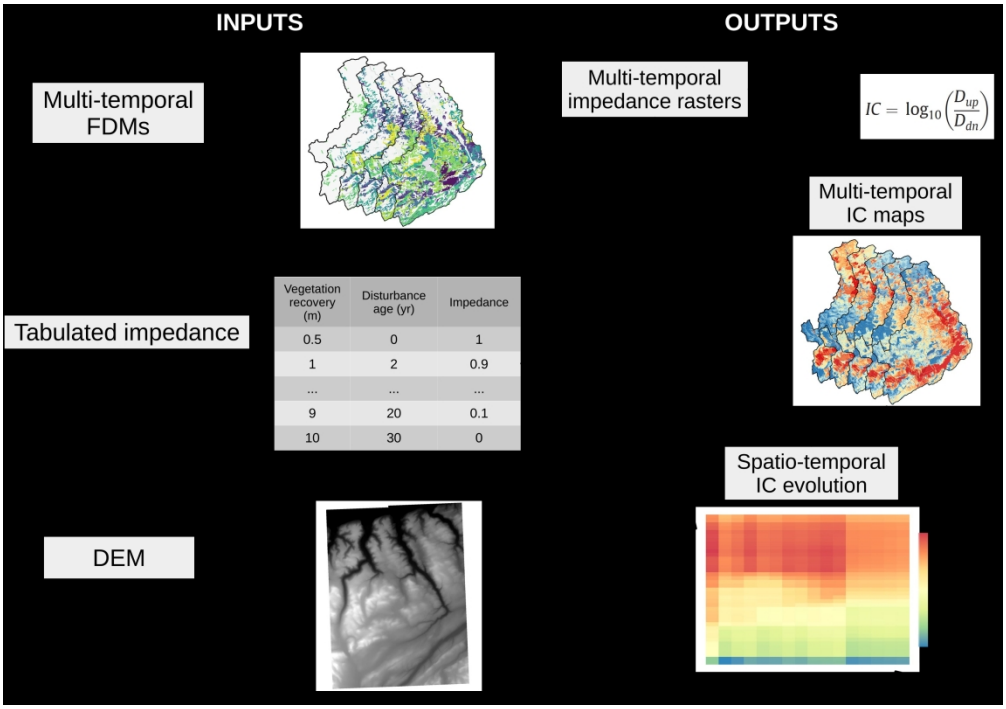


Synthetic workflow used to assess the interannual evolution of IC using FDMs, tabulated impedances and a DEM.